5. DISCUSSION OF RESULTS

The experimental data presented in Chapter 4 are grouped in two main Sections: full-scale and pilot-scale studies. The former gave evidence on the hydrodynamic behaviour, flow distortions and related process performance encountered in two full-scale anaerobic reactors commonly used for primary domestic wastewater treatment (AP and UASB). The latter yielded valuable information on modified AP configurations whose main purpose was to overcome the hydrodynamic inefficiencies and process removal limitations encountered in the full-scale reactors. Thus, the concept of the high-rate anaerobic pond (HRAP) for the advance primary treatment of domestic wastewater arises from combining the best features of two well-established technologies: a conventional low-rate reactor (AP) and a high-rate reactor (UASB). Therefore, the last section of this chapter discusses the increased removal efficiencies found in two HRAP configurations, based on the improvements of their hydrodynamic features, enhanced biomass retention and an overall less limited mass transfer process (i.e. improved mixing and contact between substrate and biomass).

5.1 Full-scale experiments

5.1.1 Anaerobic ponds

Hydrodynamic behaviour. As pointed out by Wood (1986), the design and performance of a waste stabilisation pond (and in general of any biochemical reactor) depends substantially on two factors: an adequate description of its mixing characteristics and an adequate estimation of its biological degradation rate constant. Limitations in quantifying these two factors seem to explain the disagreement between expected and current operating performance data on full-scale WSP.

The sludge profiles plotted in Figures 4.1 and 4.4 show very different accumulation patterns in the two AP. This demonstrates that the geometry of the pond, as well as the relative positioning of inlets and outlets, greatly affects the patterns of sludge deposition. The settling pattern of sludge at Ginebra formed a U-shaped channel along the pond, whereas at Toro the sludge formed a wide top inverted cone (funnel shaped). Peña *et al.* (2000) pointed out that findings of this sort show that the dynamic interactions between water movement (advection phenomena) and the biosolids layer may play an important role in the location of in-pond methanogenic zones (i.e. sludge

accumulation zones), settled solids resuspension and the consequent variations of effluent quality in terms of COD, BOD_5 and suspended solids.

Figures 4.2 and 4.3 display the sludge profiles obtained after partial desludging of the AP at Ginebra. Interestingly, during the initial tracer experiment at Ginebra (53% sludge accumulation), the biogas bubbling was always observed around the middle zone of the pond where a high accumulation of sludge also occurred. The observed bubbling pattern consisted of large biogas outbursts whose intensity and frequency seemed to increase after 0900 h reaching its maximum at around noon on a sunny day. This qualitative observation is in agreement with results reported by Toprak (1995b) on the biogas production pattern in the AP at Sesimbra in Portugal. More recently, a research project carried out at the Western Treatment Plant (close to Melbourne, Australia) showed that biogas production zones were also located at half-length of a rectangular AP (Warren, 1998). Sludge samples from these active zones yielded higher counts of methanogenic archaea compared to other zones of the pond. Thus, there seems to be a correlation between sludge settling zones and concurrent anaerobic digestion processes.

In contrast, during the following tracer experiments at Ginebra (30% and 20% sludge contents respectively) the main biogas production zone disappeared from the middle of the pond and was replaced by a more evenly distributed swarm-like bubbling. This new biogas bubbling pattern was observed in the last two thirds of the AP. Meanwhile, in the AP at Toro the large biogas outbursts were always present in both tracer experiments. Their location, however, changed slightly from the opposite embankment (in relation to inlet-outlet) towards the centre of the AP when the inlet positioning was changed.

The RTD curve in Figure 4.5 (a) showed an early sharp peak indicating significant short-circuiting during the preliminary tracer experiment at Ginebra. The RTD curve in Figure 4.6 (53% sludge accumulation), however, showed a more arbitrary flow pattern with mixed and dead volumes coexisting within the AP (Levenspiel, 1999). Differences in the responses from these two consecutive tracer experiments were evident despite that sludge volume was still the same and flow rate figures were similar. Nevertheless, the preliminary experiment started at 1300 h when sunlight and biogas bubbling were intense, whereas the next dispersion study started at 0800 h when neither sunlight nor biogas bubbling were significantly strong. Although tracer dispersion depends primarily on advection phenomena (flow movement) it may also be affected by the intensity of biogas bubbling, which in turn depends on environmental variables such as temperature and sunlight intensity.

The RTD curve for 30% sludge contents showed a higher peak value (E_{peak} = 2.4) compared to the maximum (E_{peak} = 2.0) in the 53% sludge accumulation experiment. According to Levenspiel (1999), the type of curve obtained for the 30% sludge accumulation shows a slow internal circulation and suggests inadequate mixing along with sluggish slow turnover of fluid. Additionally, the peak value was obtained earlier in this curve (θ = 0.05) compared to the 53% sludge contents (θ = 0.12) despite that mean flows and differences between influent and effluent temperatures were similar in both experiments (Peña *et al.,* 2000). Wind blew against the main flow line with a frequency of 95% in the first experiment (53% sludge contents), but this frequency was reduced to only 53% in the second experiment (30% sludge contents). Hence, the predominant wind direction might explain the lower peak value and the higher peak delay obtained in the first experiment.

On the other hand, the tracer experiment for a 20% sludge accumulation showed a substantially reduced peak value (E_{peak} = 1.1) compared to the previous experiments, but it was also obtained earlier (θ = 0.11). It is also worth noting that the inflow rate during this last experiment was about half of the values recorded in the previous experiments (i.e. 10.3 l/s, 18.5 l/s and 19.3 l/s for 20%, 30% and 53% sludge contents, respectively). Meanwhile, temperature variations remained within the same range whilst wind blew against the flow line with a frequency of 45% in this last experiment.

All the RTD curves from the full-scale AP at Ginebra showed that most of the tracer left the pond early (before θ = 1.0). This is characteristic of misbehaving mixed flow reactors with a strong tendency to dead zones, some degree of short-circuiting and reduced mixed volumes (Levenspiel, 1999).

In-pond tracer concentrations determined at the surface and 1.0 m depth for the 53% sludge accumulation experiment (in-pond tracer data are shown in Appendix I and Appendix II in FULL-SCALE-EXP\AP-DISPERSION\Internalpoints.doc) showed that peak concentrations appeared first in the samples taken at 1.0 m depth. This finding suggests a preferential subsurface flow path and it is in agreement with the U-shaped cross-sectional channel found in the sludge profile. The top water layer was flowing against the wind direction most of the time (frequency of 95%) whilst subsurface layers moved faster towards the outlet as suggested by the earlier peaks obtained at the 1.0 m depth samples. Nonetheless, the absolute peak tracer concentrations both at the surface and 1.0 m depth samples were similar. Molecular diffusion took over after 32 hours of $[Li^+]$ dosage since concentrations were evenly distributed throughout the sampling points after this time.

In-pond tracer data for the 30% sludge accumulation experiment showed that peak concentration values at both surface and 1.0 m depth were similar and were also obtained at the same time with the exception of point 4 located midway on the right hand side of the AP. This new tracer spatial distribution suggests that the preferential flow path found in the previous experiment was changed after a 43% reduction of the initial sludge contents. Additionally, an evenly distributed concentration field indicates an improved overall mixing pattern within the reactor. Molecular diffusion took over after 35 hours of [Li^+] dosage in this experiment.

In-pond tracer data from the 20% sludge accumulation experiment showed a different pattern in comparison with the previous runs. The points located in the first half of the AP yielded much earlier tracer peak concentrations at 1.0 m depth compared to surface points, and the concentration values differ significantly amongst one another. Conversely, the points in the second half of the pond produced similar tracer peak concentrations and response times. Molecular diffusion in this experiment took over after 58 hours (nearly 1.7 times the period taken in previous experiments). This behaviour indicated a completely new mixing pattern in the AP after 63% of its initial sludge content was evacuated. It has to be taken into account that inflow rate for this experiment was half of the value recorded in the previous runs.

The hydrodynamic parameters in Table 4.3 showed an improvement of the mixing pattern in the AP at Ginebra once the sludge content was reduced to 30%. Both δ and HRT_e values increased, the former from 0.06 to 0.08 and the latter from 0.88 d to 0.95 d. These figures demonstrated that pond mixing improved but also that a new fraction of pond volume was incorporated to the active zone.

On the other hand, further desludging of the AP led to a smaller δ value (0.03), which seemed to promote a plug-flow like pattern. Nonetheless, the HRT_e value for this condition showed the lowest figure (1.30 d) in comparison to the maximum achievable of 3.1 d. The foundations of the dispersion model help to explain this apparent contradiction of a lesser dispersion degree along with a higher dead zone ratio and a likely short-circuiting fraction. As pointed out by Levenspiel (1999) and Bailey and Ollis (1986), dispersion is the result of molecular diffusion superimposed on the advective motion of fluid. Thus, it seems logical that if fluid kinematics takes over molecular diffusion, the spread of tracer will be small and this will result in smaller δ values, suggesting a misleading plug-flow like pattern.

Table 5.1 shows the estimation of active and dead volumes in the AP based on the RTD shape, the dispersion model results and the compartments model as

recommended by Levenspiel (1999). Although the peaks in the RTD curves indicated the presence of short-circuiting, it was difficult to estimate accurately this fraction from the plots. It is clear, however, that short-circuiting fractions in the first two experiments were small given the narrow peak bases. Likewise, short-circuiting in the last experiment seemed to be minimal as there was no well-defined peak in the response curve.

Table 5.1 Estimates of active and dead volumes in the AP.

Experiment	V_t (m^3)	V_s (m^3)	V_e (m^3)	V_a (m^3)	V_d (m^3)
Ginebra 1 (53% sludge)		1805	1632	1450	1987
Ginebra 2 (30% sludge)	3437	1033	2404	1510	1927
Ginebra 3 (20% sludge)		695	2742	1150	2287
Toro 1 (adjacent in-out)	4468	1373	3095	1300	3168
Toro 1 (diag. opposite in-out)				2280	2188

Subscripts: t, total; s, sludge; e, effective; a, active; d, dead.

$V_e = V_t - V_s$; $V_a = T_e \times Q$; $V_d = V_t - V_a$

A sharp short-circuiting from inlet to outlet was observed in the preliminary experiment at Toro as confirmed by Figure 4.5 (b). Similarly, Figure 4.7 obtained from the first experiment (original inlet-outlet positioning) showed also a large peak value (E_{peak} = 42.8) recorded after only 15 minutes of tracer dosing. This RTD shape is related to a substantial direct short-circuiting from inlet to outlet (Levenspiel, 1999). Tracer application, however, was done at the same time in both experiments and temperature variations were similar. To some extent this result appears logical given the poor inlet-outlet positioning and physical design of this AP. Wind blew in the same direction of the main flow line with a frequency of 44% during this experiment; this could enhance the short-circuiting and explain the remarkably early sharp peak and tracer washout.

In the second experiment, the modified inlet was a 250 mm diameter PVC pipe. It discharged the influent 0.50 m below top water level and was located diagonally opposite to the outlet channel. Figure 4.7 displays the RTD curve obtained with the new inlet arrangement.

The change in the inlet design and position improved the mixing pattern of the AP. Although the tracer peak was still sharp and early, its value (E_{peak} = 5.2) was about one ninth of the peak value obtained with the original inlet-outlet positioning. Both δ and HRT_e values increased, the former from 0.04 to 0.07 and the latter from 1.0 to 1.2 d. This result is positive taking into consideration that the mean flow rate during the second experiment (modified inlet arrangement) was 57% higher than that in the first

experiment (original inlet-outlet arrangement). Temperature variations and wind conditions (speed and direction) were fairly similar for both experiments.

On the other hand, in-pond tracer data for the first experiment showed that peak [Li^+] concentrations first occurred at the surface points. Nonetheless, the difference in concentrations between surface and 1.0 m depth samples was not significant with the exception of points 4 and 6. In contrast, maximum tracer concentrations were obtained at the same time at both surface and 1.0 m depth points during the second experiment; and concentration values were also similar. Thus, the modified inlet arrangement reduced the preferential flow path and enhanced overall pond mixing. The latter can be confirmed by the diffusion pattern, which took over 15 hours later in the second experiment compared to the first. Such delay could have been related to a new fraction of the pond incorporated into the active volume.

The dispersion numbers calculated from the RTD experimental curves provided evidence of large deviation from plug flow since all values were higher than 0.01. These results are in agreement with the findings reported by Marecos do Monte and Mara (1987) for primary and secondary facultative ponds in Portugal. Hence, the hydrodynamic behaviour of these two AP falls in the category of a misbehaving CSTR as discussed by Levenspiel (1999). Mass balances performed on the effluent (*C, t*) data series yielded a recovery of [Li^+] of 79, 78 and 52% at Ginebra and 89-96% at Toro. The very low [Li^+] recovery for the last experiment at Ginebra also confirmed the increased dead volume shown by the RTD and the data in Table 5.1.

The experimental HRT values (HRT_e) in Ginebra were around 33-43% of the theoretical values, whilst in Toro HRT_e figures accounted for 29 to 50% of the theoretical ones. Table 5.1 shows that despite desludging increases the effective volume of the pond by releasing space occupied by sludge, the increase in active volume is much more smaller as shown by V_a values for the first two experiments. Surprisingly, further desludging of the pond at Ginebra increased the dead volume and reduced the active fraction of the reactor. Two factors may explain this loss in hydrodynamic efficiency: first, the biosolids contents of the AP induce mixing by biogas bubbling, despite sludge itself occupying some of the physical volume of the AP. Secondly, as the inflow rate in the last experiment was low (only 50% of the average values in the two previous runs), the incoming water jet had much less kinetic energy available to produce free turbulence and hence mixing in the bulk of fluid volume. This process of free turbulent mixing by incoming jet interaction with stationary fluid is known as entrainment and is described by Massey (1998).

The AP at Toro evidenced an important recovery of active volume by adjusting the design and positioning of the inlet. It is worth noting that V_a increased by 75% and V_d decreased by the same amount in the second experiment (in which the sludge volume was the same as in the first experiment). This improvement in the overall mixing pattern was also achieved with a higher flow rate. Since the new inlet was a submerged pipe, it produced an incoming jet within the AP, which was completely different from the surface channel discharge in the first experiment. It seems, therefore, that improved hydrodynamic efficiency in this case was due to the combined effect of adequate inlet positioning and enhanced free turbulent mixing induced by the incoming water jet (Massey, 1998).

Process performance. Table 5.2 presents the main operational parameters of both AP during the tracer studies. The APs were always underloaded ($\lambda_a < \lambda_t$) and their mean BOD_5 removal efficiencies were often below the expected value of 60% for the operational temperatures recorded. The only exceptions were the second experiment at Ginebra (BOD_5 removal of 66%) and the first experiment at Toro (BOD_5 removal of 68%).

Table 5.2 Operating parameters of the AP during the experiments.

Experiment	T	Q	V	Volumetric organic loads ($gBOD_5/m^3$ d)			
	(°C)	(m^3/d)	(m^3)	λ_d	λ_t	λ_a	λ_r
Ginebra 1	23	1668		118	300	149	85
Ginebra 2	22	1598	3437	118	300	101	67
Ginebra 3	21	890		118	300	70	35
Toro 1	25	1261	4468	118	300	79	54
Toro 2	24	1979		118	300	152	74

Subscripts: d, design; t, theoretical based on Mara et al. (1992); a, applied; r, removed.

Mean total COD removal efficiencies presented in Table 4.5 for Ginebra AP showed small variations between the first two experiments (61 and 59%). Nevertheless, mean total COD removal fell to 21% in the last experiment (20% sludge accumulation). BOD_5 and TSS removals improved in the second experiment (30% sludge contents) compared to the first but decreased again when sludge contents was reduced to 20%. Comparison of the effluent BOD_5 and influent settled BOD_5 (Imhoff cone supernatant) proved that the AP removes part of the suspended and dissolved organic matter fractions in the influent. The mean effluent BOD_5 concentrations in the first and second experiments (sludge accumulations of 53 and 30%) were 57 and 44% of the mean influent settled BOD_5 concentrations respectively. In the third experiment, however, the

mean effluent BOD_5 accounted for 75% of the mean influent settled BOD_5. Thus, a decrease in the removal efficiency of part of the suspended and dissolved organic matter fractions may explain the increase in the proportion of effluent BOD_5 to settled BOD_5 during the third experiment at Ginebra when sludge contents in the AP was only 20%.

COD removal in the AP at Toro showed practically the same trend for both conditions (before and after inlet changes), whereas TSS removal improved markedly after the inlet layout was changed. The average effluent BOD_5 in the first experiment was about 74% of the settled BOD_5 influent concentration, but this figure increased to 76% in the second experiment (new inlet layout). These figures remained practically the same and showed that the fractions of suspended and dissolved organic matter removed in the AP at Toro was lower compared to the AP at Ginebra. This fact suggests that sludge accumulation has a higher impact on the overall effluent BOD_5 reduction than the positioning of inlet-outlet devices.

On the other hand, the average COD/BOD_5 ratios in the influent for each experiment at Ginebra and Toro were 1.8, 1.6, 1.5 and 1.8, 1.6 respectively. These figures show the high biodegradability of the wastewaters produced in both towns.

Statistical correlations. Multiple linear regressions by least squares method were performed on the data series shown in Table 4.4. Data from the experiments carried out at Ginebra yielded statistically significant correlations between influent and effluent COD, HRT_e values, influent and effluent TSS and the inverse of the dispersion number (i.e. the Peclet number, $Pe = 1/\delta$).

Peclet number is a dimensionless group that characterizes the intensity of mixing (i.e. $Pe = 0$ for complete mixing and $Pe = \infty$ for plug flow). Any value of Pe between these two extremes shows an arbitrary flow pattern and large values of Pe are the result of non-extensive mixing within the reactor (Bailey and Ollis, 1986). As pointed out by Treybal (1981), Pe is also a useful parameter to quantify mass and heat transfer phenomena under specific conditions. In the current work, however, Pe will be only used to quantify mixing intensity within the reactors evaluated.

On the other hand, data series from the experiments at Toro did not yield statistically significant correlations for any combination of variables since the coefficient of determination (R^2) was always less than 0.50. Equations 5.1 and 5.2 are the multiple linear regression models obtained from data at Ginebra.

The lack of statistically significant correlation between physicochemical parameters at Toro AP may be related to the few runs (only two) performed on that pond. Additionally, the two-week period between the inlet changes and the second

experiment may have been too short and so the pond was not yet in steady state in terms of hydrodynamics and process performance.

$$\frac{COD_e}{COD_i} = 0.927 - (0.666/\theta) + 0.012Pe \quad (5.1)$$

where: COD_e = COD effluent (mg/l)

COD_i = COD influent (mg/l)

Pe = Peclet number (Pe = 1/δ)

θ = Experimental HRT (d)

Multiple R = 0.956
R^2 = 0.914
Adjusted R^2 = 0.895
Standard error = 0.065

$$TSS_e = 0.829TSS_i + 99.395\theta - 178.75 \quad (5.2)$$

where: TSS_e = TSS effluent (mg/l)

TSS_i = TSS influent (mg/l)

Pe = Peclet number (Pe = 1/δ)

θ = Experimental HRT (d)

Multiple R = 0.905
R^2 = 0.819
Adjusted R^2 = 0.779
Standard error = 61

The evidence gathered in these experiments shows that sludge accumulation in AP and inadequate inlet-outlet positioning strongly affected the hydrodynamics and overall process performance in the two full-scale AP at Ginebra and Toro. Excessive sludge accumulation causes operational inefficiencies related to loss of active volume. On the other hand, it would seem that total desludging of the pond is not good either because efficiency drops dramatically; this indicates that the AP has to effectively restart once completely desludged. Consequently, there seems to be threshold levels (minimum and maximum) of sludge accumulation that compensate for hydrodynamic inefficiencies and it is suggested that mixing induced by biogas bubbling may cause the

compensation effect. The smaller concentrations of effluent BOD_5 compared to influent settled BOD_5 support this argument because mixing and contact are the main mechanisms responsible for soluble organic matter removal (Pavlostathis and Giraldo-Gomez, 1991). The sludge layer is a dynamic component, whose interactions with the supernatant water affect the overall removal efficiency of AP. Results reported by Saqqar and Pescod (1995) and more recently by Paing *et al.* (2000) and Nelson and Jimenez (2000) support this argument. Hence, efficient settling of suspended organic matter and subsequent anaerobic digestion of the settled sludge bring about mixing and contact of the water column contents with the active biomass via biogas bubbling intensity. The adequate coupling of these mechanisms explains the higher organic matter removal efficiencies of APs compared to conventional settling units.

On the other hand, the relative positioning and type of inlet-outlet arrangement also affect the hydrodynamic pattern and efficiency of AP, as suggested by Mara *et al.* (1992). The results obtained suggest that diagonally opposite inlet-outlet positioning, together with submerged inlet piping, intensifies mixing in the AP volume. This effect, combined with mixing due to biogas bubbling may improve dissolved organic matter removal. However, the data obtained in this respect were not conclusive and further research is needed on this aspect.

Overall hydrodynamic behaviour of the two full-scale AP studied herein showed the mixing pattern of a misbehaving CSTR with coexistence of short-circuiting and dead zones. The multiple linear correlation model described by Equation 5.1 shows the general form of a CSTR with first order kinetics where substrate removal is a function of $(1/\theta)$; the theoretical model shown in Equation 2.40 predicts this same behaviour. The second term in Equation 5.1 takes into account the mixing and dispersion factors since the Peclet number ($Pe = 1/\delta$) is a dimensionless group that quantifies these phenomena (Treybal, 1981). The statistical correlation parameters also confirm the adequacy of a CSTR-like model.

The distortions of the CSTR model displayed by the two AP are related to, and influenced by the sludge contents and their dynamics as well as the positioning and type of inlet-outlet devices. Thus, it seems sensible to develop engineering interventions such as baffling and compartmentalization aimed at controlling the random effects of sludge dynamics and improving mixing and contact patterns throughout the effective volume of conventional AP. In this sense, Section 5.1.2 discusses the applicability of CFD modelling as a tool to study different alternatives for the hydrodynamic improvement of full-scale AP.

5.1.2 CFD modelling of anaerobic ponds

Model calibration and verification. This is probably the most important stage of a CFD modelling study because its success will depend on the amount and quality of data available to set up the CFD model (DHI, 1995).

The sludge profile shown in Figures 4.9 (a) and 4.10 depicts the main settling areas of the pond. The particulate material settled out along the left and right hand sides of the AP in a 5 m wide strip, whereas sludge accumulation in the central part of the pond was much less. The settling pattern is undoubtedly related to the prevailing hydrodynamic conditions in the AP (Vega, 2001).

On the other hand, the experimental work carried out at Ginebra found a U-shaped cross-sectional channel that suggested a subsurface preferential flow path along the centre of the pond. Figure 4.9 (b) shows the velocity field obtained for the calibration run in the AP. The flow pattern simulated with the CFD package MIKE 21 exhibited a complex behaviour with a heterogeneous velocity field including internal recirculation zones, stagnant zones (velocities close to zero) and short-circuiting regions (high velocities compared to the bulk of the AP). Likewise, the calibration run showed clearly the existence of a preferential flow path with the highest velocities occurring in the inlet-outlet flow line. Meanwhile, the lowest velocities occurred at the sides of the AP and these coincided with the zones of higher sludge accumulation. These results are in close agreement with experimental data presented in the previous section and also with the findings reported by Sanchez (2001). Wood e*t al.* (1998) found similar results in a facultative pond whose flow pattern was dominated by a relatively high velocity inlet fluid jet; these results were obtained from a 2D-CFD simulation using FIDAP 7.52 package applied to experimental data reported by Mangelson and Watters (1972).

Flow data for the Ginebra AP were entered into the model both as a variable (recorded data series) and as a constant average value. In both cases the recorded experimental values and simulated inflow rates varied from 15 to 20 l/s.

Water levels difference higher than 0.6 cm between inlet and outlet zones of the AP produced calculation instabilities that affected the numerical solution of the simulations. The average experimental difference in water levels of around 0.1 cm did not produce instabilities and water flow calculations were satisfactorily completed.

The Manning-Strickler roughness coefficient (k) was tested as a constant average value for the whole AP and as a variable figure depending on the sludge profile, type of particles (i.e. cohesive or non-cohesive) and location within the calculation mesh. The latter allowed the handling of different values for k as a function of water

depth (DHI, 1995). The best hydrodynamic approximation to experimental data was found with variable *k* figures. Hence, the value of *k* (used for the calibration and further simulations) decreased as a function of water depth. Table 5.3 shows the *k* values for different sludge depths and cohesive sludge particles (DHI, 1995).

Table 5.3 Roughness coefficient as a function of sludge depth.

k **($m^{1/3}/s$)** *	**H (m)**
48	> 3
32	2 - 3
16	< 2

* *k* (= 1/*n*) is known in central Europe as the Strickler coefficient (the inverse of Manning's time space roughness coefficient), and it should have the dimensions [$L^{1/3}$ T^{-1}] so that Manning's equation becomes dimensionally homogeneous (Massey, 1998).

The wind direction was set as blowing predominantly (80 percent of the time) from the W-NW direction, that is, against the inlet-outlet flow line. This wind direction was in agreement with historical records from nearby hydrometeorological stations and on-site measurements reported by Vorkas and Lloyd (2000). Wind speed was fixed at 1.5 m/s (Cenicaña, 2000) and the wind friction coefficient at 0.0026. The value of the latter parameter produced steady conditions throughout the AP and was in agreement with figures recommended in the MIKE 21 user's manual (DHI, 1995).

The application of CFD modelling tools to WSP is a relatively new field of work. There are very few studies carried out and reported in the literature in relation to this topic (Shilton, 2000). Nonetheless, mathematical modelling has been used for many years to solve hydraulic and hydrological problems such as tidal studies, river hydraulics, modelling of water distribution networks, sewerage systems and runoff. The application of new modelling tools to WSP hydrodynamics began in the mid 90's with the advent of modern computing technology. An early paper published by Gu and Stefan (1995) reported the results of a CFD modelling study performed on three WSP located at Minnesota (USA). In this case a dynamic lake water quality model (MINLAKE) was modified and applied to the three ponds. This study was aimed at studying thermal stratification in the water column and its dynamics as a function of weather fluctuations and the inflow jet entrainment and mixing. The calibration of this model was done based on pond morphology, meteorological data and inflow/outflow data series (Gu and Stefan, 1995). This work did not have a high requirement of data input since the CFD package MINLAKE was a one-dimensional model. The ability and therefore complexity of a CFD model to perform simulations close to real scenarios

increases with the number of dimensions included in the space-time calculation mesh (1D, 2D or 3D).

Wood *et al.* (1995) carried out a CFD modelling of a hypothetical rectangular facultative pond in order to explore the application of a commercial CFD package (FIDAP 7.0) to simulate in-pond flow patterns. Once the CFD package was tested on the simple rectangular configuration, it was used to simulate first the effect of an inlet baffle and then another baffle positioned at the outlet. This study did not include a validation step as the results presented were only aimed at showing qualitatively the potential application of CFD. These authors, however, stressed the importance of validation and calibration studies as a prerequisite to obtain sensible results applicable to real situations. In this sense, the CFD modelling outputs presented in this work are regarded as a reasonably good prediction of real flow patterns in ponds since calibration and validation of MIKE 21 were based on velocity values and dispersion data determined experimentally in the same AP (Peña *et al.,* 2000; Sanchéz, 2001; Vega, 2001).

Some researchers have pointed out the inappropriateness of using 2D-CFD packages for the modelling of WSP hydrodynamics. Wood *et al.* (1998) concluded that 3D-CFD simulations of ponds is the most suitable strategy to describe properly the effect of different inlet arrangements. Nevertheless, these authors did not discuss factors such as roughness coefficient, pond base (biosolids layer) profile, wind effects and flow variations, which altogether determine the fitness to reality of the model's output.

Shilton (2000) modelled a facultative pond by using PHOENICS 3D-CFD package. This study concluded that CFD had potential for pond design, although further research was needed on the modelling itself as well as on the collection of field data for validation purposes. This author also pointed out that with more rigorous experimental fieldwork the validation step could be confidently achieved.

Previous experiences on CFD modelling applied to WSP suggest that availability and quality of experimental data are key components to calibrate and validate any CFD package, regardless of its complexity (whether 1D, 2D or 3D). It is also clear that the amount of data and computational power requirements increase with the number of space coordinates (1D > 2D > 3D) (Wood *et al.,* 1998; Shilton, 2000).

Figure 4.12 shows that simulated RTD curves conformed better to experimental values when adopting δ values as a function of flow velocity. Peters *et al.* (1998) point out that dispersion variation depends on the spatial correlation between velocities. This assumption makes good physical sense since flow velocities are variable throughout the

pond and this influences the spread of the tracer (which is inherent in the dispersion model). Experimental and simulated tracer peak values (C/C_o from 0.90 to 1.00) were obtained at t/HRT_t values of 0.15 to 0.20; this is a reasonably good match for experimental and simulated figures taking into consideration previously published results with a wider variation (Wood *et al.,* 1995; Wood *et al.,* 1998).

Simulation runs. Simulation runs were carried out for the current configuration of the full-scale AP at Ginebra (1456 m^2 surface area and 4 m depth). The modelling results given in Figures 4.13 to 4.18 and Table 4.6 account for hydrodynamic and dispersion phenomena due to water movement only. Any additional advection and mixing effects due to biogas released from the AP sludge layer were not considered, as MIKE 21 does not incorporate specific kinetic expressions for anaerobic digestion. The simulations were run on the configurations depicted in Figure 3.1.2.

Sludge effects. Figure 4.13 shows the impact of a high sludge accumulation (50% sludge volume) on the velocity field that causes a jet current from inlet to outlet. This trend was also confirmed by the RTD curve of configuration A in Figure 4.15 (E_{peak} = 1.6). A medium sludge accumulation (30% sludge volume) yielded a more even velocity distribution with slightly higher velocity values as shown in Table 4.6. Configuration C (desludged pond) presented an even velocity distribution throughout the pond but increased velocity values. This apparent contradictory trend of higher velocities for lower sludge accumulations may be explained by a smaller roughness coefficient in the absence of sludge. Thus, lower frictional resistance allows a faster flow. Velocities were small in all cases (1.8-4.0 x 10^{-3} m/s), however, the channelling effect was again confirmed by higher velocity values towards the centre of the pond as shown in Table 4.6.

Configuration B (30% sludge volume) has an E_{peak} of 1.4 whereas the desludged pond (Configuration C) showed an RTD curve closer to the ideal CSTR model with an E_{peak} of 1.1. Simulated and experimental BOD_5 removal efficiencies were similar for configuration A, but differed in the case of configuration B. The latter may explain the positive impact of an adequate amount of active biosolids on the performance of AP. The CFD package was unable to model this situation, as it would require specific kinetic rate expressions for anaerobic biodegradation processes. However, the model was able to estimate reasonably well the removal for configuration A because it has such a high sludge accumulation that total efficiency was low due to physical reduction of the pond's active volume. Similarly, a misleading interpretation of the small δ values for A and B would suggest flow patterns close to PF. However, taking into

consideration that dispersion is the result of molecular diffusion superimposed on the advective motion of fluid (Levenspiel, 1999), an alternate explanation is that the drag caused by channelling effects did not allow a broad tracer spread and small δ values were obtained as a result. This can be another way of interpreting small δ values in reactors prone to short-circuiting. On the other hand, the retention factor improved as sludge contents decreased, thus showing an increase in hydrodynamic efficiency.

Inlet-outlet positioning and baffling. Inlet-outlet arrangements were simulated as the on-site situation (i.e. aligned along the longitudinal centre line of the pond) and also in diagonally opposite corners. Baffles were positioned across the AP with a total length equal to two thirds of the pond width. The effect of the baffles was to cut the main flow path established between the inlet and the outlet. Baffles increased flow velocities in the first compartment, but redistributed the velocity field and values in downstream compartments (see Figure 4.16). This effect was more noticeable in aligned inlet-outlet configurations than in diagonally opposite layouts. In the latter case velocity values were more evenly distributed throughout the pond, as shown in Table 4.6. All baffled configurations, except Configuration I, produced RTD curves with E_{peak} values of around 1.0. This feature together with increasing retention factors ranging from 0.77 to 0.88, confirmed the positive impact of baffling on pond hydrodynamics. Shilton (2000) observed a similar improvement when adding a baffle in the middle of a facultative pond. In terms of BOD_5 removal efficiency the best configurations were F, H and I, with removals of 62, 62 and 65 percent respectively. The addition of two baffles to the aligned inlet-outlet layout (F) makes it as good as an adjacent corner inlet-outlet layout with a single mid-pond baffle (H). In all cases δ values showed an intermediate mixing pattern. An additional foreseeable benefit of baffling would be on the control of sludge random movement throughout the AP. These physical barriers might help the retention of settled biosolids on the first compartments of the baffled AP. This effect has been observed in the anaerobic baffled reactor with the additional advantage of separating acidogenesis and methanogenesis longitudinally down the vessel (Barber and Stuckey, 1999). Thus, the reactor may behave as a two-phase anaerobic system with acidogenic and methanogenic activities increased by a factor of up to four. This two-phase-like anaerobic reactor increases the stability of process performance. Cohen *et al.* (1980) found that acidogenic bacteria accumulate within the first compartment and methanogenic archaea in the last compartments. In this way different microbial groups can develop under more favourable environmental conditions. The latter, however, is a hypothesis for the present work that may be worthy of further research.

Pond geometry. An equivalent pond with the same surface area and depth, but with a square shape, was also modelled. The early sharp tracer peak (E_{peak} of 1.5) was reduced to a smaller value (E_{peak} of 1.1) by simply changing the positioning of inlet-outlet from an aligned layout (J) to a diagonally opposite layout (K), as shown in Figures 4.17(a), 4.17(b) and 4.18. Peña *et al.* (2000) found experimentally a significant reduction in a massive early peak in a full-scale square AP after the inlet device design and positioning with respect to the outlet was improved. Nonetheless, the results given in Table 4.6 suggest that existing square ponds with incorrect inlet-outlet arrangements can be greatly improved by simply providing a baffle at L/2 (Configuration L). Such a baffle improved the velocity field distribution (see Figure 4.17(c)), which in turn increased the retention factor up to 0.85. Consequently, greater organic matter removal efficiencies may also be expected. Intermediate mixing patterns are evidenced by the δ values obtained for all these configurations.

Figures 5.1 to 5.4 show graphically the evolution of the tracer slug simulated by MIKE 21 for θ = 0.5, 1.0 and 1.5 (θ = t/HRT$_t$). The colour code for concentration values in mg/l is as follows: yellow (C = 0.20), orange (C = 0.09), red (C = 0.08), brown (C = 0.06), dark green (C = 0.04), light green (C = 0.02), pale blue (C = 0.01) and blue (C = 0.0).

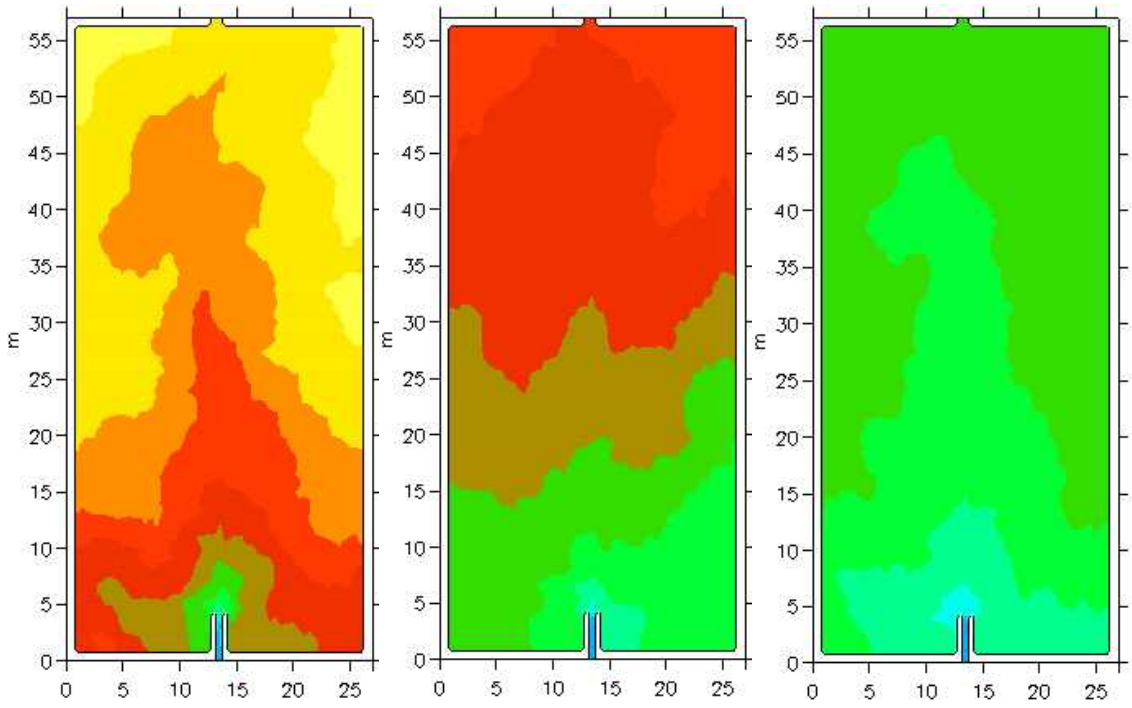

θ = 0.5 θ = 1.0 θ = 1.5

Figure 5.1 Tracer transport for high sludge accumulation and aligned inlet-outlet.

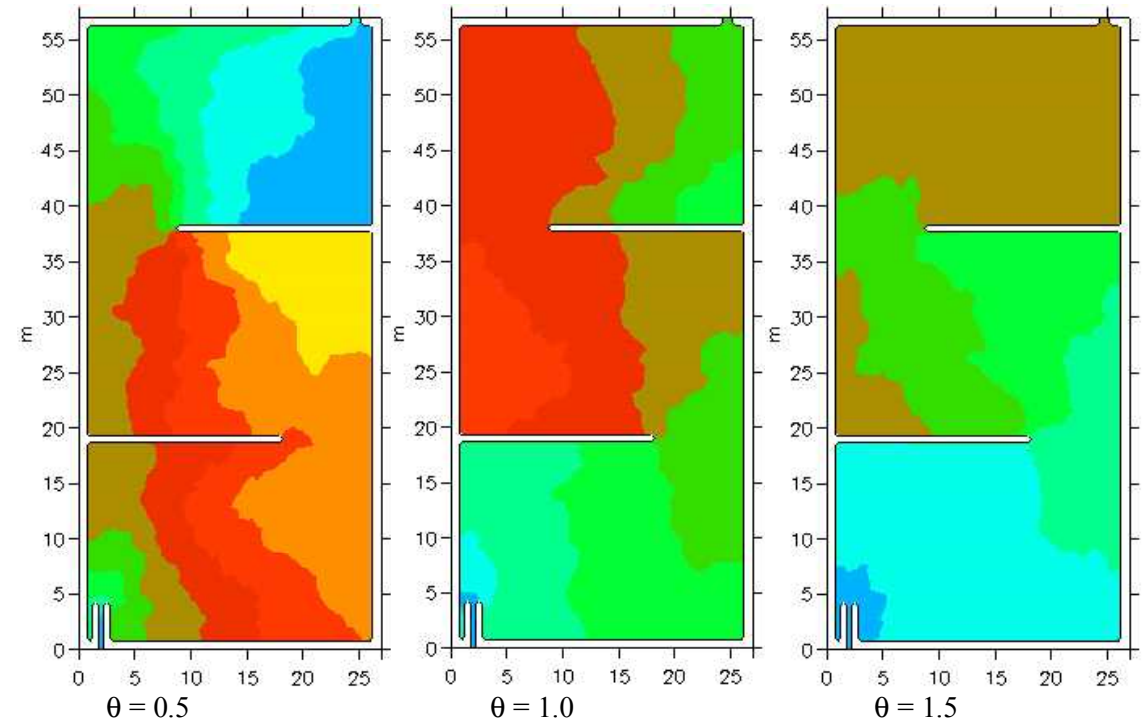

Figure 5.2 Tracer transport for desludged pond, 2 baffles and opposite inlet-outlet.

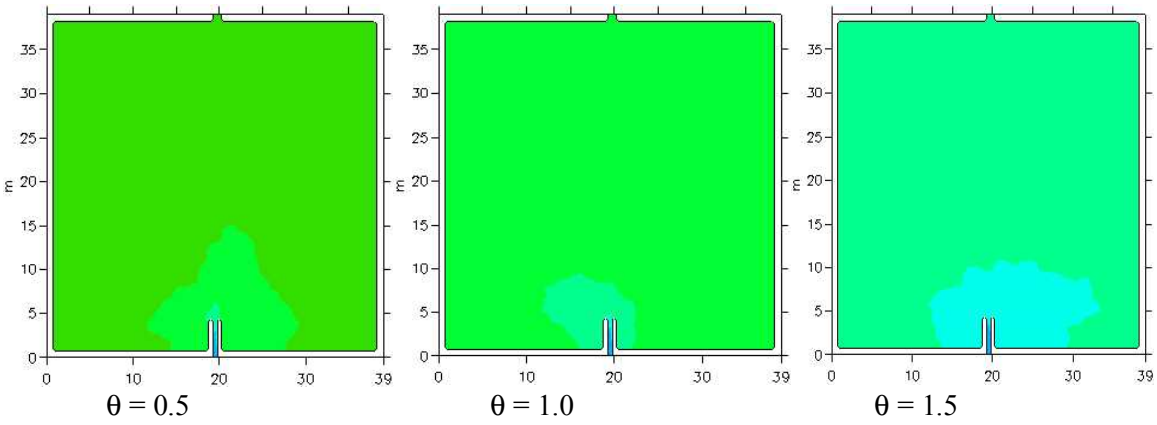

Figure 5.3 Tracer transport for square pond and aligned inlet-outlet.

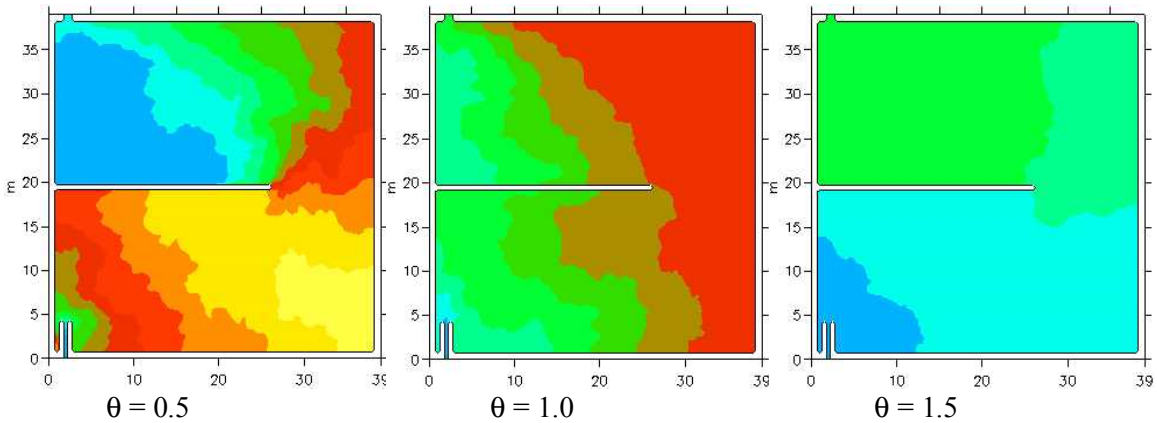

Figure 5.4 Tracer transport for square pond with one baffle.

Figures 5.1 to 5.4 confirm the numerical values presented in Table 4.6. Tracer peak concentration starts leaving the AP with 53% sludge accumulation before $\theta = 0.5$ and by $\theta = 1.0$ it has left completely. The baffling, however, improves the flow pattern and reduces the tendency to short-circuiting. The square geometry in Figure 5.3 yields a virtual tracer washout since by $\theta = 0.5$ most of the tracer has already left the pond. The baffle depicted in Figure 5.4 greatly improves the circulation pattern and hence tracer retention in the pond. The dispersion pattern in Figure 5.1 shows how at the beginning ($\theta = 0.5$) the tracer peak concentrations are transported through the middle of the pond whereas dispersion towards the sides is much slower. By the time θ equals 1.5 there is no concentration gradient present and molecular diffusion seems to predominate. Baleo *et al.* (2001) observed a very similar temporal and spatial variation in tracer dispersion in a 3D-CFD modelling study performed on a bench-scale pond by using FLUENT package. These authors argue that zones of low velocity are always present in the proximity of fluid and solid boundaries (i.e. base and sides of the pond) due to flow resistance and this creates localized inevitable dead zones.

On the other hand, it is worth noting that estimated BOD_5 removals in Table 4.6 are related solely to the improvement of advection-dispersion phenomena. Likely additional contributions of biogas bubbling to enhance mixing and contact may result in higher removal efficiencies than those predicted by the CFD package. The CFD modelling performed at Ginebra AP suggests that adequate combinations of inlet-outlet arrangements, provision of baffles and optimal geometric design of the pond may correct flow distortions found in full-scale AP. The baffling alternative seems particularly good given its expected benefits not only in terms of hydrodynamics but also of biological process performance. Most of the results and discussion presented in this section were recently submitted and presented as part of a paper in the 5th International WSP conference held in Auckland, New Zealand (Vega *et al.,* 2002).

Unlike previous studies reported in the literature, the 2D-CFD package MIKE 21 (which is a depth-integrated model) was able to predict reasonably well the hydrodynamic and advection-dispersion phenomena in ponds, provided that a careful calibration and verification stage is carried out. The inclusion of different specific parameters (e.g. water levels, wind, roughness coefficient, flow rate variations, dispersion data) and the intrinsic numerical method of implicit alternant directions (IAD) for solving the hydrodynamic and dispersion differential equations, make this model highly stable and suitable for resolving a wide range of complex environmental applications (DHI, 1995).

5.1.3 Start-up of UASB reactor

The start-up of the UASB reactor at Ginebra was an important stage prior to the hydrodynamic evaluation of the reactor under steady state conditions. Nonetheless, a thorough research and discussion of the start-up phase of UASB reactors is out of the scope of this work. Thus, this section will discuss the results obtained mainly from the perspective of achieving a good operational condition in the reactor.

Inoculum characteristics. Table 4.8 shows the characteristics of the sludge seed before commencing the start-up. By the end of the start-up the SMA increased to 0.23 gCOD-CH_4/g VS-d and the final concentration of VS and TS were 10.2 and 26.7 g/l respectively. The SMA value obtained after start-up was in agreement with figures from other UASB reactors treating domestic wastewater in tropical regions (van Haandel and Lettinga, 1994). Despite an apparent biomass loss (reduction of VS and TS concentrations) at the end of the start-up, there was, however, a substantial improvement in both SMA and biogas production. The latter increased from 12.9 to 60 l biogas/m^3 of treated wastewater once the reactor reached steady-state operational conditions.

The observed overall sludge loss may be attributed to the release of inert solids (reduction of TS) and raw organic material stored in the sludge bed as well as to the scouring of bad quality sludge particles (reduction of VS). These factors may have been related to the combined effect of transient influent flows and likely excessive sludge withdrawals from the reactor. The latter occurred just 10 days before the start-up period was finished (Rodríguez *et al.,* 2001).

Previous work reported in the literature recommend that start-up of UASB reactors for domestic sewage treatment should commence at low hydraulic loading rates (i.e. HRT of about 24 h), which must be periodically increased up to the design value (Lettinga *et al.,* 1980; Vieira *et al.,* 1994; van Haandel and Lettinga, 1994; Hammad, 1996). There are no recommendations in these publications about particular procedures to improve the quality of the sludge seed. Alphenaar *et al.* (1993) studied the effect of HRT and liquid upflow velocity on the granulation process of anaerobic sludge and the competition between different anaerobic bacterial consortia. They found that the granulation process was favoured by the combination of short HRT and high upflow velocities. These authors called the combination of these parameters the *selective pressure*. They concluded that although granulation (i.e. formation of pellets) of anaerobic sludge is a complex process related to many factors, the selective pressure

method imposed on a particular sludge is one of the crucial factors in sludge granulation processes.

The selective pressure method quoted earlier was applied to the sludge seed extracted from the AP. The central idea, however, was to improve the quality of the sludge, not to obtain granules in the UASB but mainly to enhance sludge settling properties and biochemical activity. Table 3.9 shows the combination of extreme HRT and upflow velocity values applied to the UASB once seeded and prior to continuous feeding. Meanwhile, Table 4.9 shows the combination of HRT and upflow velocities throughout the start-up phase in continuous operation.

Batch period. The organic matter present in the reactor at the beginning of the batch period was readily removed in less than 5 days. This showed that biomass selected in the sluicing stage got completely activated as evidenced from the relatively high removal rate. It is arguable whether the batch period is essential in all cases. It would seem logical that a sludge seed already adapted to the wastewater does not need a further acclimatizing period as it should be able to utilize readily the substrate. In other words, the metabolism and enzymatic reactions of the biomass are already suited to the substrate they have been feeding on. This was probably the case in this study since the inoculum was extracted from an AP that was receiving the same substrate. On the other hand, an inoculum exposed to a completely new substrate will need to readapt its enzymatic machinery to the new feed and this would result in a delay of biologically mediated removal processes.

VFA, pH and BI. The raw wastewater quality was stable along the study as demonstrated by pH values around 7.0 in all of the samples. The variation of BI shown in Figure 4.22 confirms that buffer capacity was enough to neutralize the production of VFA during the start-up period. Negative effects produced by accumulation of acidity were not observed as pH values were kept within an optimum range. These favourable environmental conditions allowed a healthy development of the bacterial groups responsible for hydrolysis, acidogenesis and methanogenesis. The final conversion of VFA into methane is supported by the low effluent concentrations of VFA recorded throughout the start-up phase (VFA 0.5-1.0 meq/l). The average effluent concentration of VFA was below 1.0 meq/l (i.e. 60 mg H-Ac/l) as shown in Figure 4.22. These values compare well with figures reported by van Haandel and Lettinga (1994) on the UASB at Pedregal, Brazil. Likewise, there was no risk of reactor acidification as shown by the BI stability. The latter is expected in the anaerobic treatment of most domestic wastewaters given their buffer capacity. The reactor showed an instability signal between days 28

and 39 (HRT = 9.8 h) since a slight accumulation of VFA occurred. Nevertheless, the reactor recovered its stability after a short period and reduced again the concentration of effluent VFA below 1.0 meq/l.

Organic matter removal. Figures 4.19 to 4.21 and Table 5.4 show the variation of COD concentrations and average removal efficiencies during the start-up phase. The effluent COD concentration was low from the beginning of start-up and showed a stable pattern (see Table 4.10). Thus, the UASB removed a considerable percentage of the applied organic load once continuous feeding started. However, most of the effluent COD corresponded to the soluble fraction indicating either a low participation of biological removal processes in the overall performance or the presence of soluble non-biodegradable organic matter. Hence, most of the removal at the beginning of start-up was mostly due to physical processes like solids entrapment, adsorption, settling and filtration. This finding is in close agreement with previous results reported elsewhere (Dean and Horan, 1995; Speece, 1996; and Droste, 1997).

The high HRT values (low hydraulic loading rates) at the beginning of the start-up produced low upflow velocities, which promoted the presence of poorly mixed zones in the reactor. Consequently, the contact between active biomass and substrate was not optimum and the biogas production was minimum. Conversely, as HRT was reduced the upflow velocities were increased and produced a better contact between biomass and substrate. A natural consequence of this was the improvement of soluble COD removal and the corresponding increase in biogas production. The latter showed the influence of upflow velocity in the overall mixing of the system. The best removal efficiencies of soluble organic matter occurred at HRT values less than 9.8 h as depicted in Figure 4.21. This means that upflow velocities higher than 0.50 m/h were beneficial to the hydrodynamic behaviour and to the biological process development and functioning in the reactor (Manzi, 2000). The performance of the UASB became more stable at HRT values less than 16 h.

An improved spatial distribution of the sludge bed and its quality were additional benefits caused by the progressive increase in upflow velocity (i.e. reduction of HRT). On the other hand, HRT values less than 7.0 h (design condition) seemed to produce washing out of sludge as shown in Figure 4.24. However, the reactor recovered quickly its previous stability and it was able to operate efficiently at a HRT of 6.7 h. It is worth noting that high upflow velocities (i.e.V_{up} > 0.55 m/h) produced sludge bed expansions above the maximum desirable limit. This factor increased the potential for sludge scouring and its consequent volume reduction for HRT less than 7.0 h.

Table 5.4 Average removal of COD, BOD_5, TSS and S. solids 1-h during start-up.

Parameter	HRT (h)					
	25	**16**	**14.3**	**9.8**	**8.3**	**6.7**
Total COD removal (%)	67	59	69	69	69	61
Maximum COD removal (%)	73	77	79	82	84	78
Filtered COD removal (%)	24	39	52	43	58	46
Total BOD_5 removal (%)	66	N.D	78	82	79	79
TSS removal (%)	78	74	74	67	69	59
Settleable solids 1-h (%)	98	98	97	90	87	63

N.D = Not determined

The low variability of the UASB effluent quality even after reductions of HRT, demonstrated that the reactor could have easily started operation at a HRT less than 25.0 h. The best functioning period was obtained for a HRT of 8.3 h when average total COD removal was 69%. Average removal efficiencies of total COD varied between 59 to 69 % during the start-up period. These values are satisfactory for a domestic wastewater with high contents of particulate material. It may be argued that it was possible to shorten the start-up phase since the UASB could have been started with an HRT of 15.0 h ($V_{up} \cong 0.30$ m/h). In this way, the total start-up period would have been shortened to around 30 days.

Figures 4.23 to 4.25 and Table 5.4 show the variation and average removals of BOD_5, TSS and Settleable (1-h) solids throughout the start-up period. BOD_5 removal showed less variation than the other parameters monitored. Average BOD_5 removal efficiencies ranged from 66 to 82% and the maximum removals were achieved at stages IV and V (HRT of 9.8 h and 8.3 h) with values of 82 and 79% respectively. These figures confirmed that removal of biodegradable organic matter took place from the very beginning of the start-up and was not greatly affected by the increasing hydraulic loading rates. Based on this, it may also be argued that the selective pressure applied to the sludge seed contributed to its enhanced biological activity. The best removals of BOD_5 were obtained after stage III and these coincided with the best removals of filtered COD.

TSS and settleable solids mean removals, however, diminished steadily as hydraulic loading rates increased. The latter may be explained by sludge particles release due to sludge bed expansion caused by increasing upflow velocities and induced mixing via biogas bubbling. These effects are reported by van Haandel and Lettinga (1994) who observed that the high sludge concentration in the UASB at Pedregal dropped sharply after 10 weeks of commencing the start-up. This was attributed to an

intense biogas induced mixing that expelled poor quality sludge. Consequently, sludge particles with improved settling properties developed and remained in the sludge bed afterwards.

Sludge bed development. At the beginning of the start-up (just after the batch period) the sludge accumulated at the bottom of the reactor. It occupied only 12 % of the total reactor volume as shown in Figure 4.26. This was mostly due to sedimentation by compression (sedimentation type 4) since the reactor contents were kept undisturbed for 10 days. This sludge compaction was observed during stages I, II and III (i.e. HRT 25.0, 16.0 and 14.3 h). During the following period (i.e. HRT between 14.3 and 9.8 h) the sludge bed showed a tendency to float or move upwards as a whole unit. This phenomenon may have been related to the combined effect of sludge compaction and occluded gas within the compacted bed. Thus, a further increase in hydraulic loading rate (i.e. reduction in HRT) would help the compacted sludge bed to move upwards as a result of an increased buoyancy force. This behaviour of the sludge bed was first reported in pilot UASB reactors by Lettinga *et al.* (1980) and more recently by Dean and Horan (1995) in a UASB reactor treating combined wastewater (domestic sewage and industrial effluents) in Mauritius.

Every time sludge bed flotation occurred, the inflow was directed to only half of the feeding points so as to produce a vertical velocity gradient. This velocity gradient was able to homogenise the reactor contents and destroy the flotation tendency. This procedure allowed the release of occluded biogas bubbles and a further selection of good quality sludge particles. Consequently, the sludge bed was regrouped and responded well from this moment up to the end of the start-up phase.

However, the sludge bed was expanded during the last stage of start-up due to the upflow velocity (V_{up} = 0.64 m/h) produced by the maximum applied hydraulic loading rate (i.e. smallest HRT = 6.7 h). This expansion was most likely due to an increased biogas production recorded during this stage.

The development of the sludge bed is shown in Figures 4.26 to 4.29. Table 5.5 shows additional parameters related to sludge quality and stability. The volatile solids (VS) contents were kept relatively constant whereas total solids (TS) contents showed a slightly higher variation during the start-up as shown in Figure 4.29. Nonetheless, the parameters related to sludge quality (MA and V_s) evolved positively during the different stages of start-up.

Table 5.5 Parameters related to sludge quality and stability.

Parameter	HRT (h)					
	25	**16**	**14.3**	**9.8**	**8.3**	**6.7**
Sludge loading rate (kg COD/kg VS d)	0.09	N.D	0.15	N.D	0.26	0.31
VS/TS	0.44	N.D	0.48	N.D	0.46	0.42
V_{up} (m/h)	0.17	0.27	0.30	0.43	0.52	0.64
V_s (m/h)	3.18	N.D	3.50	N.D	4.10	3.00
SMA (g COD-CH_4/g VSS d)	0.05	N.D	N.D	N.D	0.10	0.23

N.D Not determined

Figures 4.26 to 4.29 show the dynamics of the sludge bed during the start-up. It is interesting that the sludge bed remained at the bottom of the reactor with no expansion from the beginning of continuous feeding up to the third stage (HRT = 14.3 h). The TS concentration was reduced from 113 kg TS/m^3 to 102 kg TS/m^3 as shown in Figures 4.26 and 4.27. This reduction of TS in the sludge bed was in agreement with a slight increase in effluent TSS concentration during the same period despite the low V_{up} values. The latter suggests a steady loss of poor settling particles carried away in the effluent. The sludge profiles shown in Figures 4.27 and 4.28 depict a good vertical distribution of the sludge bed with the highest TS and VS concentrations occurring in the lower section of the bed (h < 1.0 m) whereas the lowest concentrations were found at the top of the layer, that is, in the blanket (2.3 m < h <1.5 m). This sludge behaviour is in agreement with results obtained by Florencio *et al.* (2001) on a full-scale UASB reactor treating domestic sewage in Recife, Brazil.

Table 5.5 shows that VS/TS fraction was around 0.45 throughout the start-up period. Similar values were observed in full-scale UASB reactors treating domestic wastewater in Cali (Colombia) and Kanpur (India). Results from the UASB at Pedregal (Brazil) showed a VS/TS fraction of 0.55 – 0.65. The smaller VS/TS fraction found at Ginebra can probably be attributed to a higher inert material fraction in the raw wastewater. This same reason explained the low VS/TS fractions found in Cali and Kanpur reactors (van Haandel and Lettinga, 1994).

On the other hand, the sludge settling velocity showed a steady increase that seems to correlate with the increase in upflow velocity. Table 5.5 also shows that sludge settling velocities were much higher than upflow velocities and this ensures that most of the sludge particles will remain in the reactor. Nonetheless, bioflocs with poor settling properties will be inevitably carried away in the effluent. The slight increase in effluent TSS concentration supports the loss of poor settling particles and thus the reasonably small variation of sludge contents, as shown in Figure 4.29.

SMA values in Table 5.5 showed a good evolution throughout the start-up. Nonetheless, the SMA determined prior to continuous feeding (SMA = 0.19 g COD-CH_4 / g VS d) was substantially reduced to a value of 0.05 g COD-CH_4 / g VS d once feeding of the reactor started. The final value of SMA at the end of start-up (0.23 g COD-CH_4 / g VS d) was even higher than the SMA value obtained prior to continuous feeding (i.e. after sludge seed was selected). Therefore, the increase in upflow velocities and sludge loading rate helped to recover and improve the initial biochemical activity of the sludge achieved after the selective pressure procedure.

The sludge loading rate was low at the beginning of the start-up but after stage III it fell within current recommendations for UASBs treating domestic wastewater (PROSAB, 1999; van Haandel and Lettinga, 1994).

On the other hand, the SMA value achieved at the end of the start-up compares well with published results by Lettinga *et al.* (1981), Grin *et al.* (1983), Schellinkhout *et al.* (1985) and Barbosa and Sant'Anna (1989), which were in the range 0.10-0.25 g COD-CH_4 / g VS d for anaerobic treatment of domestic wastewater in UASB reactors.

Biogas production. Figure 4.30 shows the evolution of biogas production during the start-up. These data support the gradual activation and development of the anaerobic bacterial consortia needed. Biogas production achieved its maximum rate after a HRT of 14.3 h. Based solely on biogas production, it could be said that the optimal operation point of the UASB at Ginebra corresponded to a HRT value somewhere between 14.0 and 8.3 h.

Although specific parameters of the anaerobic process microbiology were not measured, the positive correlations between COD removal efficiency, biogas production, SMA values and the stability of the control variables (i.e. pH, T, BI, Alkalinity) demonstrated that the start-up period allowed the healthy development of all anaerobic bacteria and archaea groups needed to treat the wastewater. Furthermore, the results of SMA and sludge settleability at the end of the start-up period confirmed the overall improvement of the anaerobic sludge quality. Therefore, the selective pressure seemed to be an adequate procedure to improve poor quality and flocculent anaerobic sludge seeds with the consequent benefits for a more stable and shorter start-up period under full-scale conditions.

Statistical correlations. Linear regressions were performed on different parameters. Significant correlations were found between contents of VS within the reactor and total COD removal, removed organic load and biogas production, upflow velocity and sludge bed expansion. The statistical correlations are shown in Figure 5.5.

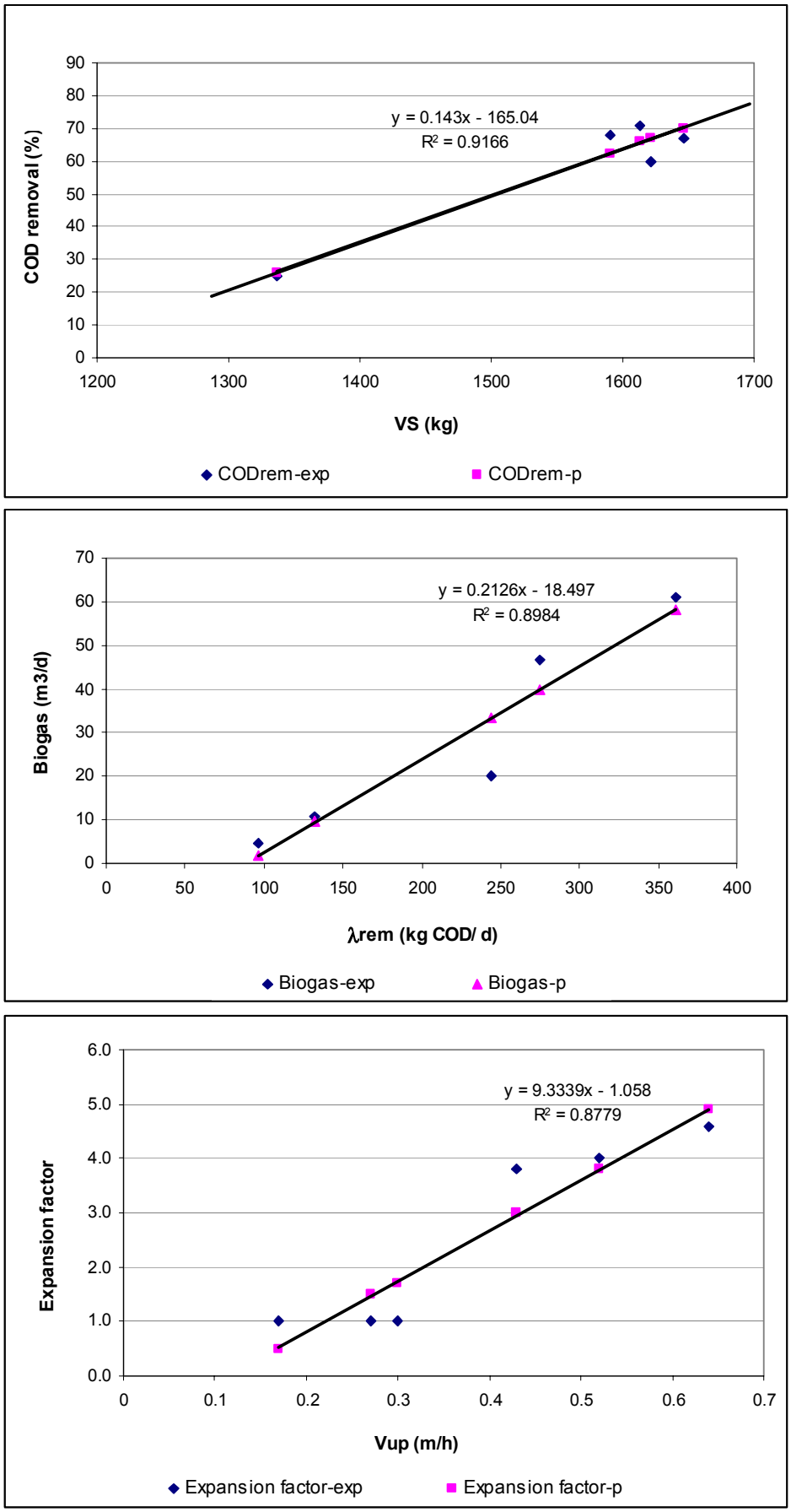

Figure 5.5 Statistical correlations between operational parameters and biological process variables.

Figure 5.5 shows a direct positive correlation between VS contents and total COD removal as evidenced by R^2. However, it has to be said that given the natural dispersion of the data for these two parameters, a good correlation would always be observed. As hydraulic loading rate increased, so did the COD removal. It is therefore expected that part of the organic matter removal ends up as new biomass within the reactor which contributes to VS contents. Although it is nearly impossible to distinguish the nature of the VS contents (whether cells or fresh organic matter), this correlation confirmed a logical trend between sludge bed growth and organic matter removal.

Biogas production also increased as a result of improved organic load removal. This direct correlation ($R^2 = 0.898$) also confirms that there was an increase in biomass contents and activity because there is no other way to obtain stable end products (biogas) in the anaerobic digestion process. Nonetheless, the specific biogas production obtained at Ginebra (slope of the correlation line: $Q_b = 213$ l biogas/kg COD removed) was lower than theoretical figures given in the literature.

Using Equation 3.8 with a mean wastewater temperature of 25 °C (see Table 4.7), a biogas recovery factor ($f_m = 0.60$) and a partial pressure of methane of 0.80 (at K= 298), the theoretical biogas production would be $Q_b^* = 286$ l biogas/kg COD removed. The measured biogas production at Ginebra was 75% of the theoretical production figure. This difference is explained by likely biogas losses since the top of the reactor was not covered during the start-up.

The last plot in Figure 5.5 shows a linear correlation between upflow velocity and sludge bed expansion ($R^2 = 0.878$). From this relation it can be seen that for every increase in V_{up} there will be a proportional expansion of the sludge bed. However, the bed expansion is also highly related to biogas production rate (Heertjes and Van der Meer, 1978). High biogas production rates can negatively affect the start-up since sludge aggregates may be pushed towards the top of the reactor and be washed out with the effluent (PROSAB, 1999). This was not a real problem during the start-up period; however, special attention should be paid to an excessive expansion of the sludge bed to avoid a detrimental loss of biomass.

The start-up phase of the UASB at Ginebra was developed satisfactorily and the methodology applied confirmed its advantages by shortening the start-up period to only nine weeks. The selective pressure procedure (i.e. step-wise increase of upflow velocity) proved to be an effective method to select the sludge with best settling properties. Consequently, lower volumes of sludge seed (inoculums) with poor quality can be used to start-up an UASB reactor in short periods of time.

5.1.4 Hydrodynamic study of UASB reactor

Overall hydrodynamic behaviour. Before discussing the RTD curves and hydrodynamic parameters, it is worth noting that the stability of pH, temperature and hydraulic loading rates presented in Tables 4.11 and 4.12 insured good experimental conditions for each tracer run and its replicate. The hydraulic loading rate varied more (CV = 0.29) in the first run compared to the rest of the tests. Apart from this the conditions were very even throughout the whole experiment.

The hydrodynamic behaviour of full-scale UASB reactors has been comparatively less studied than organic matter removal processes. Nonetheless, the degree of conversion in any bioreactor depends on both its hydrodynamic behaviour (i.e. mixing properties) and the rate of conversion at which biological reactions occur (Levenspiel, 1999). Moreover, UASBs are three-phase reactors, which receive a complex substrate with dissolved, suspended and particulate matter. This situation makes it necessary to improve the understanding of UASB hydrodynamic behaviour.

The overall hydrodynamic behaviour of the reactor can be analysed from the RTD curves obtained at the effluent. Figure 4.31 shows the RTD curves for the theoretical HRT tested (10, 8, 6 and 5 h). Every plot displays the experimental RTD and its duplicate along with the theoretical CSTR curve.

RTD curves obtained for stages 1 and 2 according to Table 4.12, showed the typical shape of a misbehaving mixed reactor with dead zones. E_{peak} values of 1.50 and 1.40 were obtained for HRT_t values of 10.6 and 7.8 h respectively. These curves also show that most of the tracer left the reactor before $\theta = 1.0$. This feature and the steep and early descending branches of the RTD curves confirmed the UASB reactor had a fraction of its total volume in dead space (Levenspiel, 1999). The duplicates of the RTD showed smaller peak values in comparison (E_{peak} 1.20 and 1.00) but the early and sharp descending branches of the curves remained equal.

On the other hand, the peak values higher than unity (E_{peak} >1.00) show that there was also a short-circuiting flow between inlet and outlet.

RTD for stages 3 and 4, however, display an improved overall mixing in the UASB. E_{peak} values decreased to 1.17 and 0.97 for HRT_t values of 5.7 and 4.9 h, respectively. The descending branches of the experimental RTD got closer to the CSTR theoretical curve and this same trend was observed in the duplicates. Thus, dead zones were minimized and the short-circuiting flow seemed to disappear during the last two conditions since E_{peak} values were around 1.0.

The hydrodynamic parameters yielded by the dispersion model in Table 4.13, showed that δ values increased as HRT_t decreased. This demonstrates that mixing intensity increased within the reactor with raising hydraulic loading rates. The latter shows that mixing is affected by changes in liquid upflow velocity. Nonetheless, biogas production is another variable that contributes to mixing intensity in the sludge bed and blanket of UASB reactors (Heertjes and Van der Meer, 1978; Heertjes and Kuijvenhoven, 1982; Samson and Guiot, 1985; Bolle *et al.,* 1986).

Table 5.6 summarises the retention factor ($\beta = HRT_e/HRT_t$), δ values, liquid upflow velocity, sludge and blanket height (H_{sb}) and estimated biogas production rate (Q_b) obtained in the experiment.

Table 5.6 Summary of hydrodynamic parameters and variables affecting mixing.

Stage	Run	β	δ	Pe = 1/δ	V_{up} (m/h)	H_{sb} (m)*	Q_b (m^3/h)**
1	1	0.66	0.163	6.1	0.38	1.2	1.6
	2	0.59	0.145	6.9	0.41	1.4	3.1
2	1	0.63	0.197	5.1	0.52	1.9	2.2
	2	0.68	0.185	5.4	0.51	1.9	3.8
3	1	1.01	0.720	1.4	0.70	2.6	4.8
	2	1.10	0.591	1.7	0.71	2.6	6.4
4	1	0.88	0.355	2.8	0.83	3.2	5.7
	2	0.94	0.406	2.5	0.79	3.1	5.1

* Sludge plus blanket height estimated from correlation in Figure 5.5.
** Biogas production rate estimated from organic load removal at each run using correlation in Figure 5.5 and Equation 3.8.

The plots in Figure 4.31 show that the overall hydrodynamic behaviour of the UASB reactor was characterised by a dispersed flow pattern with coexisting mixed and dead volumes. This holds true if the reactor is underloaded or, in other words, when the operational HRT is more than the design HRT.

On the other hand, as the hydraulic loading rate approaches the design value (i.e. operational HRT equal to or greater than the design HRT), the overall hydrodynamic pattern converged to a CSTR model. Therefore, flow distortions such as dead volumes, short-circuiting and bypass flows were minimised as depicted in the last two plots in Figure 4.31.

Since the UASB is a three-phase reactor, the interaction of liquid-solid-gas influences mixing. Iliuta *et al.* (1998) argue that gas flow rates especially in the bubble flow regime together with low liquid flow velocities (V_{up} < 30 m/h) affect dispersion and hence mixing intensity, which in turn affects the Peclet number. This might be the

case in UASB reactors where biogas bubbles travel through the sludge bed and blanket together with the liquid phase moving at low velocity.

Hydrodynamic behaviour of sludge bed and blanket. Figures 4.32 to 4.35 and Table 4.14 show the RTD curves and hydrodynamic parameters obtained at internal points 1, 2, 3 and 4 as shown in Figure 3.8.

The hydrodynamic parameters together with the application of the compartment model as described by Levenspiel (1999) are useful to analyse the data from the internal points. Table 5.7 shows the retention factor ($\beta = HRT_e/HRT_t$), total (V_t), active (V_a), and dead (V_d) volumes calculated at each internal point (i.e. sludge bed plus blanket) and for the whole reactor.

Table 5.7 Estimates of active and dead volumes in the UASB reactor.

Stage and run		**1**		**2**		**3**		**4**	
Point		**1**	**2**	**1**	**2**	**1**	**2**	**1**	**2**
Effluent	V_t	275 m^3							
	V_a	182	162	173	187	275	302	242	256
	V_d	93	113	102	88	0	-27	33	19
Point 1	β	0.93	0.75	0.86	1.0	1.1	1.2	1.2	1.1
	V_t	43 m^3							
	V_a	40	32	37	43	47	52	52	47
	V_d	3	11	6	0	-4	-9	-9	-4
Point 2	β	0.92	0.74	0.60	0.76	0.92	1.0	0.90	0.94
	V_t	43 m^3							
	V_a	39	32	26	33	40	43	39	40
	V_d	4	11	17	10	3	0	4	3
Point 3	β	0.85	0.75	0.65	0.82	0.97	1.1	0.87	0.97
	V_t	43 m^3							
	V_a	36	32	28	35	42	47	37	42
	V_d	7	11	15	8	1	-4	6	1
Point 4	β	0.87	0.80	0.82	0.96	1.1	1.2	1.1	1.1
	V_t	43 m^3							
	V_a	37	34	35	41	47	52	47	47
	V_d	6	9	8	2	-4	-9	-4	-4

$V_a = T_e \times Q$ or $V_t \times \beta$; $V_d = V_t - V_a$; all volumes are expressed in m^3.

The β values obtained in the reactor outlet and internal points show the same general trend. The smaller values of β for the first two stages showed at higher fraction of dead zones for these runs and their duplicates in all internal points. Despite the β values being higher compared with the figures for the whole reactor, there was still a fraction of dead zones in the sludge bed and blanket volumes. Table 5.7 displays the

active and dead volumes calculated for the whole reactor and for the volumes corresponding to each internal point.

Again, as the hydraulic loading rate approaches the design value (i.e. operational HRT equal to or greater than the design HRT), the overall hydrodynamic pattern in the sludge bed and blanket approaches a CSTR model. The negative values in Table 5.7 mean an active volume higher than the actual physical volume (since $\beta > 1$). This does not have of course a physical meaning but it is rather a direct consequence of the geometry of the RTD curves, which is affected by the sludge dynamics. The RTD plots that yielded negative V_d values have descending branches above the theoretical CSTR model and so they comprise a larger area under the curve. Consequently, the value of their first momentum (centroid) is shifted towards the right of the expected theoretical value ($\theta = 1$) as stated in the dispersion model. According to Levenspiel (1999), a late response curve indicates either an incorrect estimation of the inflow rate or reactor volume or non-inert tracer.

An alternate explanation for smaller shifts to the right of the theoretical value ($\theta = 1$) is given by the compartment model when bypass flow coexists with a mixed volume. In this case, the estimation of the mean experimental HRT can yield a slightly higher value than the theoretical figure. Similar results were reported elsewhere by Avella (2001) and Seereeram (2001) working on anaerobic sludge bed reactors.

Mass balances performed on the effluent (*C, t*) data series yielded average [Li^+] recoveries of 71, 62, 94 and 87% for runs 1, 2, 3 and 4 respectively. The lower recoveries of [Li^+] in the effluent during the first two runs and their duplicates, confirm the presence of dead zones in the reactor. However, by checking the values of V_d estimated for the overall reactor and the sludge bed and blanket zone, there seems to be a missing additional V_d not accounted for, particularly in the first two runs. Table 5.8 presents the figures to discuss this point further. The total reactor volume is 275 m^3.

Table 5.8 Estimation of V_d values for the whole reactor volume.

Stage and run	1		2		3		4	
	1	2	1	2	1	2	1	2
Total V_d	93	113	102	88	0	0	33	19
V_d (sludge+blanket)*	20	42	46	20	4	0	10	4
Deficit/Surplus	73	71	56	68	-4	0	23	15

* Calculated as the sum of the V_d values for internal points.

Effective depth = 4.0 m, Sludge bed and blanket depth ≅ 2.5 m, Remaining depth = 1.5 m.
The negative figures in Table 5.7 were taken as zero for the calculations in Table 5.8.

Control samples of sludge and effluent taken prior to each tracer run showed undetectable [Li^+] concentrations at all sampling points.

The total reactor volume can be split into two main volumes: sludge and blanket zone volume ($V_{sb} \cong 170$ m^3), and the remaining volume ($V_r \cong 105$ m^3) corresponding to the upper part of the reactor as shown in Figure 5.6.

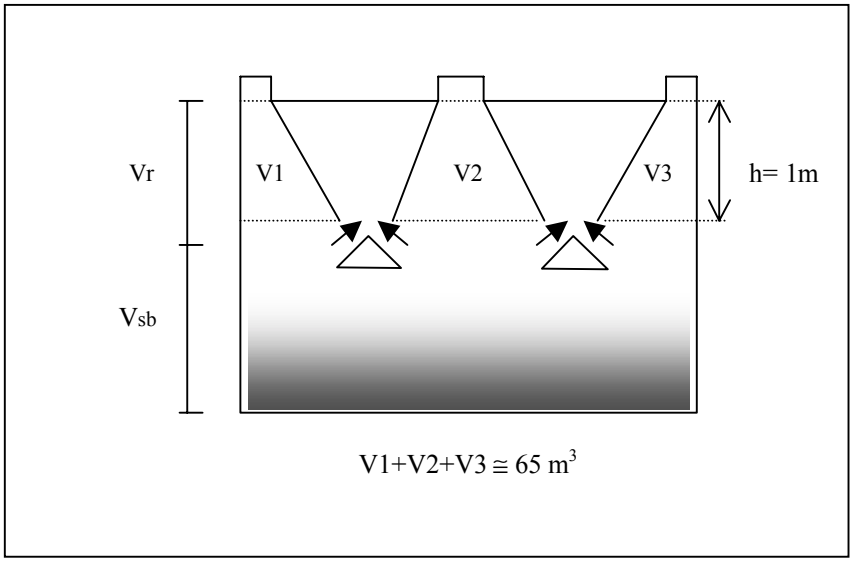

Figure 5.6 Estimation of volumes within the UASB reactor at Ginebra.

Figure 5.6 shows that water volumes contained below the gas-liquid-solid (GLS) separator device accounts for 65 m^3 based on the reactor geometry. It is worth noting that previous studies reported in the literature on the hydrodynamics and modelling of UASB reactors (Heertjes and Van der Meer, 1978; Heertjes and Kuijvenhoven, 1982; Van der Meer and Heertjes, 1983; Samson and Guiot, 1985; Bolle *et al.,* 1986) did not take into consideration the effect that water volumes below the GLS may have on the overall hydrodynamic behaviour of the reactor.

Based on the figures in Table 5.8 it is suggested that the unbalanced dead volumes (deficit) in stages 1 and 2 may be related to the likely stagnant zones shown in Figure 5.6 (V_1, V_2 and V_3). There is a good agreement between the deficit figures and the 65 m^3 value ($V_1+V_2+V_3$). In contrast, during stages 3 and 4 the dead volumes were much smaller (zero in stage 3) and this correlates well with improved mixing in the whole reactor caused by greater liquid upflow velocities and biogas production rates.

The authors mentioned above, with the exception of Samson and Guiot (1985), analysed and discussed the results of the overall hydrodynamic behaviour of a 30 m^3 UASB reactor by means of the compartment model and the cumulative dimensionless F-curve described by Levenspiel (1972). They did not estimate the difference between

the overall V_d value and the corresponding V_d values for the sludge bed and blanket zone. Moreover, the F curve integrates changes and yields a smooth line that may well hide real effects within the reactor (Levenspiel, 1999). The combination of the two factors mentioned above was probably the main reason in the quoted studies to miss the contribution of GLS below water contents to the overall dead volume. It seems, at least intuitively, that such water volumes are prone to hosting dead zones given their expected poor circulation pattern mainly at low hydraulic loading and biogas production rates. Since this factor was not directly evaluated in this study either, it is something that may be worthy of further research.

Bolle *et al.* (1986) pointed out that bypass flows and short-circuiting are a function of sludge height and they recommend a value between 3.5 and 4.0 m. Heertjes and Kuijvenhoven (1982) found, however, that the sludge height should be between 1.5 to 2.5 m to control bypass flows. Conversely, sludge heights less than 1.0 m promoted a large short-circuiting of the influent that affected the removal efficiency of the reactor. Heertjes and Van der Meer (1978) found that an increase in the sludge height above 1.8 m resulted in an improved efficiency, but also in an increased bypass flow over the sludge bed. The results presented here are in agreement with the findings of the latter authors with respect to the short-circuiting fractions in the first two stages as discussed earlier. Moreover, the negative figures for V_d in Table 5.7 obtained for stages 3 and 4 (i.e. sludge heights > 2.6 m) confirmed the existence of bypass flows over the sludge bed. The run 2 in stage 3 showed bypass flows at three internal points (negative figures) and these seemed to affect the whole reactor given the negative overall V_d figure estimated from the RTD at the outlet.

All the experimental data obtained at the internal points (i.e. sludge bed and blanket volume) showed variations among each other, despite the influent distribution device having been designed and constructed according to the recommendations given in the literature (van Haandel and Lettinga, 1994). The variations observed suggest that likely unsteady flow conditions occurred within the reactor and these may have caused disturbances in the sludge bed and blanket. During some runs it was observed that flow from some of the V-notch weirs feeding some of the pipes, trapped air and induced transient flows at some feeding points. This may be one of the factors that caused the differences in results for internal points and it was also an external source of error.

The dispersion and compartment models applied to study the hydrodynamic behaviour of the reactor showed a dispersed flow pattern with coexistence of a mixed fraction, dead zones and short-circuiting for underloading conditions. The dead volumes

were located in the sludge and blanket zones but the results also suggest that water contents underneath the GLS have the potential to host a major dead zone not reported previously in the literature.

On the other hand, the hydrodynamic behaviour improved dramatically once the reactor operated close to its design conditions. Under these circumstances the UASB closely approached a CSTR model with only a small dead zone (< 5% V_t). This result agrees well with hydrodynamic studies carried out in other UASB reactors treating domestic wastewater in Cali, Colombia (Haskoning, 1989; van Haandel and Lettinga, 1994; Correa, 1997). After a further increase in hydraulic loading rate (i.e. shorter HRT) dead zones appeared again (V_d = 10% V_t), along with bypassing flows in the sludge and blanket volume. Hence, the overloaded reactor showed a predominant mixed volume along with an intermediate dead zone plus bypass flows in its lower part. Correlations suggested in the studies quoted in this Section between the hydrodynamic behaviour, sludge height, liquid upflow velocity and biogas production were also confirmed in this research. A discrepancy between the results presented here and the mixing models reported in the literature is related to the flow pattern in the settler. Heertjes and Van der Meer (1978) and Heertjes and Kuijvenhoven (1982) reported a fraction of 5% of the total reactor volume as the plug flow zone. These authors had initially assumed that there was a plug flow zone in the settler, that their experimental F curves did not show any conclusive evidence for this. The various experimental curves obtained in this work do not show a plug flow-like fraction in the settler of the reactor at Ginebra.

Given the dynamic interactions between the three phases coexisting in UASB reactors, it seems unlikely that the settler compartment remains isolated from the turbulence occurring in the lower parts of the reactor. As pointed out by Iliuta *et al.* (1998), turbulent mixing in three-phase reactors is caused not only by liquid velocity, and other factors such as gas bubbling, but also changes in flow direction throughout the flow path and kinetic energy transfer among phases contribute to local turbulence which in turn affects mixing and contact. Thus, adequacy of a model to describe reasonably well specific hydrodynamic phenomena is an important factor that needs to be considered at an early stage. This work has shown that the coupling of dispersion and compartment models seems to provide an adequate tool to describe the macro-mixing properties of different reactor configurations.

Process performance. The composition of the raw wastewater given in Table 4.15 varied during the first two stages of the hydrodynamic evaluation due to storm

events. The dilution effect, however, did not have a serious impact on reactor efficiency as depicted in Figures 4.36 - 4.39.

On the other hand, there was a sharp increase in the average effluent concentration of all the parameters after the first run of stage 2. The mean effluent COD_t concentration remained relatively constant after the second stage, whereas the mean effluent COD_f concentration decreased steadily up to the first run of stage 4, although an increase in mean effluent COD_f concentration was recorded during the last run of stage 4. The average removal efficiency of COD_t remained relatively constant (at around 53%) after stage 2, whereas the average COD_f removal efficiency displayed a steady increase from 45 to 61% from stage 2 up to the first run of stage 4. The final removal efficiency recorded during stage 4 for this parameter was 55%.

TSS and settleable solids effluent concentrations showed an increasing trend as HRT decreased along the experiment. The increase in effluent concentrations for these two parameters was more noticeable after the first run of the second stage and this may explain the steady decrease of COD_t removal during the same period. The TSS effluent concentration increased from 81 mg/l at the beginning of stage 2 up to 180 mg/l at the end of the last stage. The settleable solids increased from 0.5 ml/l up to 1.7 ml/l in the same period. COD_t removal remained relatively constant despite the relatively high increase in effluent TSS and settleable solids. This may have been due to the steadily increasing removal efficiency of COD_f mentioned above which counterbalanced the negative effect of effluent TSS and settleable solids.

It is worth noting that the best removal efficiencies for COD_t and COD_f were achieved between the end of stage 2 and the beginning of stage 4, when the hydrodynamic performance of the reactor showed a close pattern to the CSTR model. The improvement of COD_f removal efficiency could only be achieved through better mixing and contact in the reaction zone (i.e. sludge bed and blanket).

Thus, improved mixing and more efficient mass transfer processes (i.e. enhanced transport of substrate from the bulk liquid to the microbial aggregates) can be expected as the combined result of advection and biogas induced mixing (i.e. combination of liquid upflow velocity and biogas production rate).

The removal efficiencies for most of the parameters throughout the hydrodynamic study were lower compared to the values obtained during the start-up phase. COD_f was the exception since its removal efficiency was better during the hydrodynamic evaluation.

TSS and settleable solids removal efficiencies were higher during the first two stages. This was to be expected since at low hydraulic loading rates the UASB may behave as an efficient settler and filter. Hence, particulate material is efficiently removed under such conditions (Dean and Horan, 1995; van Haandel and Lettinga, 1994). The removal efficiencies of these two parameters decreased during the last stage, that is, at the highest hydraulic loading rate. This drop in efficiency might have been influenced by an excessive expansion of the sludge bed and blanket. Table 5.6 shows that H_{sb} was around 3.1 m in the last stage and this value was high enough to push the sludge blanket to within the lower part of the settler compartment. Thus, a higher flux of particles could have left with the effluent and produced the drop in TSS and settleable solids removal efficiency.

Average COD_t removal efficiencies varied from 49 to 65% throughout the study, and COD_f removal varied from 45 to 64%. TSS removal fluctuated between 37 to 65% and settleable solids removal varied from 42 to 85%. The removal efficiencies of COD_t found in this experiment compare well with data reported in the literature for UASB reactors working under similar environmental conditions and loading rates. Haskoning (1989) reported total COD removal efficiencies between 62 to 67% in a pilot-scale UASB reactor treating domestic wastewater in Cali, Colombia. Vieira and Garcia (1991) found COD_t removals between 32 to 65% in an UASB at Sao Paulo, Brazil. Haskoning and Euroconsult (1990) found COD_t removal efficiencies between 60 to 70% in the UASB at Kanpur, India. Collazos (1986) reported a COD_t removal efficiency varying from 65 to 72% in a pilot-scale UASB reactor located in Bucaramanga, Colombia. More recently, Monroy *et al.* (2000) reported figures on COD_t removal efficiencies of several UASB reactors treating domestic wastewater in Mexico. Their data present a variation range between 55 to 75% for reactors with similar environmental and loading rate conditions to those reported herein.

The removal efficiencies of TSS reported in these studies were between 45 to 80%, with the highest frequency occurring in the range 65 to 75%. TSS removal efficiencies found in the present study were at the lower limit of figures previously published and were also lower than the data obtained during start-up phase as reported in the previous section. Hence, it would seem that operation and maintenance of the UASB in the seven-month period between start-up and hydrodynamic evaluation could affect the steady state conditions reached just after the start-up of the reactor.

Removal of microbiological indicators. The low removals of FC found in the UASB reactor at Ginebra are in agreement with the few data available in the literature

on this topic. Removals of FC varied from 21 to 79% during the whole experiment. The highest removal efficiency was achieved at stage 3 for the best hydrodynamic condition in the UASB.

On the other hand, helminth egg removal efficiency varied between 89 to 94%, and there seemed to be no direct relation between this parameter and HRT or hydraulic loading rates. The lowest removal efficiency was obtained at the last stage of the study, when the sludge blanket was more expanded. Dixo *et al.* (1995) argue that removal of helminth eggs and other particulate matter in UASB reactors are removed via filtration and aggregation through the sludge blanket. Therefore, it seems logical that removal efficiency of this parameter is affected by the degree of expansion in the sludge blanket. Consequently, the greater the sludge bed expansion the lower the removal efficiency may be. Figures in Table 4.17 show a steady drop in helminth eggs removal efficiency as HRT decreased (i.e. as sludge blanket expansion increases).

Data presented in Table 4.17 are in agreement with the average removal efficiencies of 65-80% for FC and 82-90% for helminth eggs reported by van Haandel and Lettinga (1994) and Dixo *et al.* (1995). It is clear from the microbiological point of view that effluents from UASB reactors need further treatment if reuse alternatives are to be considered.

Statistical correlations. Multiple linear regressions by the least squares method were performed on the data shown in Table 5.6 and the data series given in Appendix II in the file FULL-SCALE-EXP\UASB-TRACER-DISPERSION. Equation 5.3 is the multiple linear regression model obtained for Peclet number (i.e. mixing intensity) as a function of upflow velocity and biogas production rate. Figure 5.7 displays the correlation between experimental and predicted values of Pe using Equation 5.3.

$$Pe = 10.301 - 8.396V_{up} - 0.299Q_b \qquad (5.3)$$

where: V_{up} = Liquid upflow velocity (m/h)

Q_b = Biogas production rate (m^3/h)

Multiple R = 0.899
R^2 = 0.809
Adjusted R^2 = 0.732
Standard error = 1.101

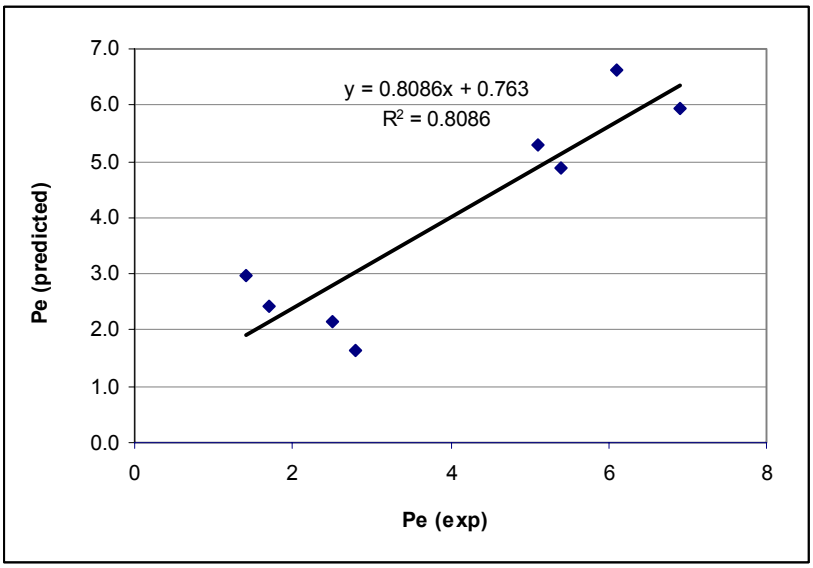

Figure 5.7 Correlation between experimental and predicted values of Pe.

Equation 5.3 shows a statistically significant correlation between Pe number, liquid upflow velocity and biogas production rate. Consequently, Figure 5.7 shows a close correlation between experimental and predicted Pe values. This result confirms that both liquid upflow velocity and biogas production rate influence strongly the mixing pattern of UASB reactors. As the hydraulic loading rate increases, the volumetric organic loading rate also increases and this results in higher biogas production rates. Therefore, the mixing intensity (i.e. Pe values or δ values) also increases and higher removal efficiencies can be attained as a result of an improved external mass transfer process within the reactor (Harper and Suidan, 1991).

Table 5.9 displays the operational parameters of the UASB reactor during the hydrodynamic evaluation. The values of V_{up}, λ_v and Q_b in Table 5.9 all showed an increasing trend during the experiment.

Table 5.9 Operational parameters during the hydrodynamic study of the UASB.

Stage	Run	Flow (m^3/h)	HRT_e (h)	V_{up} (m/h)	λ_v applied* (kg COD/m^3 d)	λ_v removed* (kg COD/m^3 d)	Q_b (m^3/h)
1	1	26	7.0	0.38	0.74	0.39	1.6
	2	28	5.8	0.41	1.15	0.76	3.1
2	1	35	4.9	0.52	0.97	0.55	2.2
	2	35	5.4	0.51	1.81	0.96	3.8
3	1	48	5.8	0.70	2.26	1.19	4.8
	2	48	6.3	0.71	2.73	1.60	6.4
4	1	56	4.3	0.83	2.88	1.43	5.7
	2	54	4.8	0.79	2.58	1.28	5.1

* λ_v = Volumetric organic loading rate.

Equation 5.4 is the multiple linear regression model obtained for the effluent concentration of TSS as a function of influent TSS concentration and experimental HRT values. Figure 5.8 shows the correlation between experimental and predicted values of effluent TSS using Equation 5.4.

$$TSS_e = 777.458\frac{1}{\theta} + 0.443.TSS_i - 135.922 \qquad (5.4)$$

where: TSS_e = Effluent TSS (mg/l)

θ = Experimental HRT (h)

TSS_i = Influent TSS (mg/l)

Multiple R = 0.903
R^2 = 0.815
Adjusted R^2 = 0.74
Standard error = 27.3

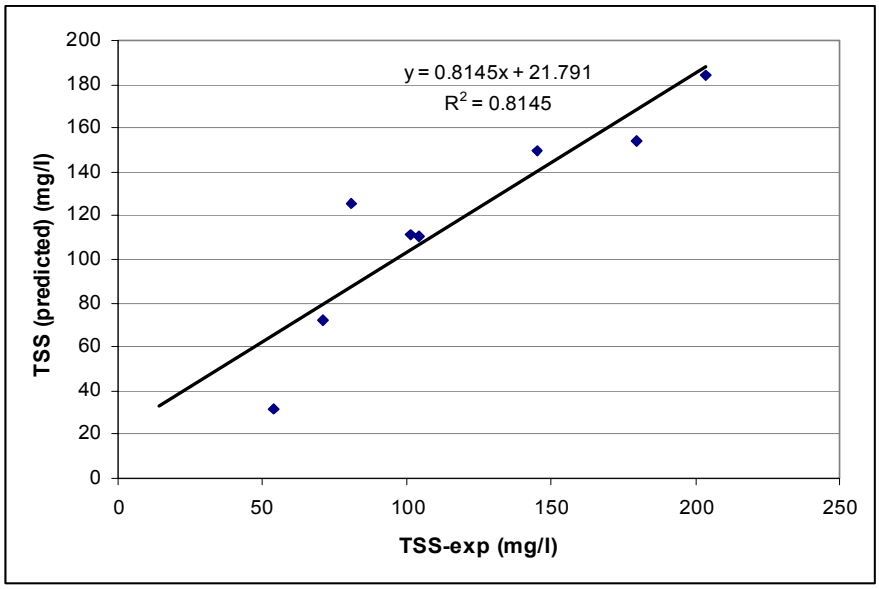

Figure 5.8 Correlation between experimental and predicted effluent TSS values.

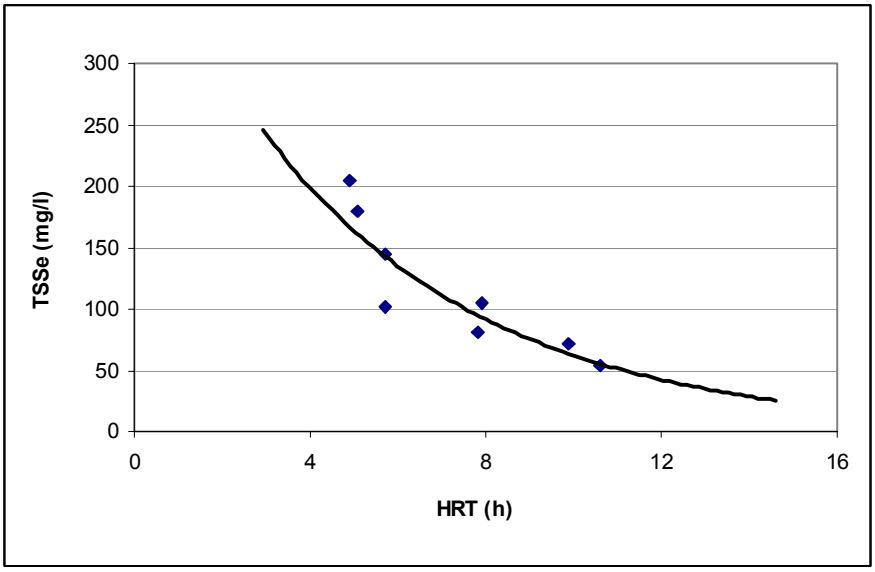

Figure 5.9 Effluent TSS concentration as a function of HRT.

Figure 5.9 shows the decay of effluent TSS concentration with HRT values. A similar trend was observed and reported by Chernicharo *et al*. (1999) with data from four UASB reactors treating domestic wastewater in different towns of Latin American countries. The UASB at Ginebra started releasing excessive TSS concentrations at HRTe < 7.0 h as shown in Figure 5.9. This, together with some regular releases of large sludge agglomerates observed in the effluent, confirmed that full-scale UASB reactors still have some problems with sludge retention efficiency in the settler.

The data on process performance showed that the UASB had its best operating condition during stage 3. At this stage, the UASB operated closest to its design conditions and was able to handle a volumetric organic load between 2.3 and 2.7 kg COD/m^3 d at an average HRT_e of 6.0 h. The volumetric organic load removed was between 1.2 and 1.6 kg COD/m^3 d. The release of TSS in the effluent from this stage onwards contributed to a smaller degree of total COD removal, although filtered COD removal was slightly higher from this stage onwards. Additionally, the hydrodynamic pattern of the UASB during this period was very close to the CSTR model and its internal mixing correlated well with liquid upflow velocity and estimated biogas production rates.

COD data modelling. Influent and effluent average COD_t data were applied to the dispersion and reaction model proposed by Wehner and Wilhelm (1956) and also to the CSTR model with first-order reaction kinetics (Levenspiel, 1999) (Equations 2.39 and 2.40, respectively). The application of these models to the COD_t data series allowed the estimation of the overall first-order reaction constants and their adequacy to describe the overall performance of the reactor.

The value of k obtained for the dispersion and reaction model was $k = 0.172\ h^{-1} \pm 0.028\ h^{-1}$ whereas for the CSTR model with first-order reaction kinetics it was $k = 0.228\ h^{-1} \pm 0.050\ h^{-1}$. These k values correspond to a mean temperature of 23 °C. The dispersion and reaction model yielded a smaller value of k but the correlation between experimental and predicted COD_t values was better with this model compared to the CSTR. Castillo *et al.* (1999) found a first-order reaction constant $k = 0.245\ h^{-1} \pm 0.002\ h^{-1}$ for CODt in a pilot UASB treating domestic wastewater at temperatures of 18-20 °C. These authors calculated k with the CSTR model and Monod kinetics. The figure obtained in this research compares well with the k value reported by Castillo *et al.* (1999).

However, no reference was found in the literature that provides k values for the dispersion reaction model proposed by Wehner and Wilhelm (1956). Despite this model

being an analytical solution of the equations of transport and dispersion phenomena for any reactor configuration exhibiting first-order kinetics and any type of inlet-outlet conditions, its application to environmental engineering problems has been rather limited. The biggest limitation of this model probably is its requirement of known dispersion number values (δ), in order to predict the effluent substrate concentration. This was not a limitation in this study as δ values were measured under different conditions.

Figure 5.10 shows the statistical correlations between experimental and predicted values of effluent COD_t for the two models mentioned above. Equations 5.5 and 5.6 show the adjusted models taking into account the experimental *k* values.

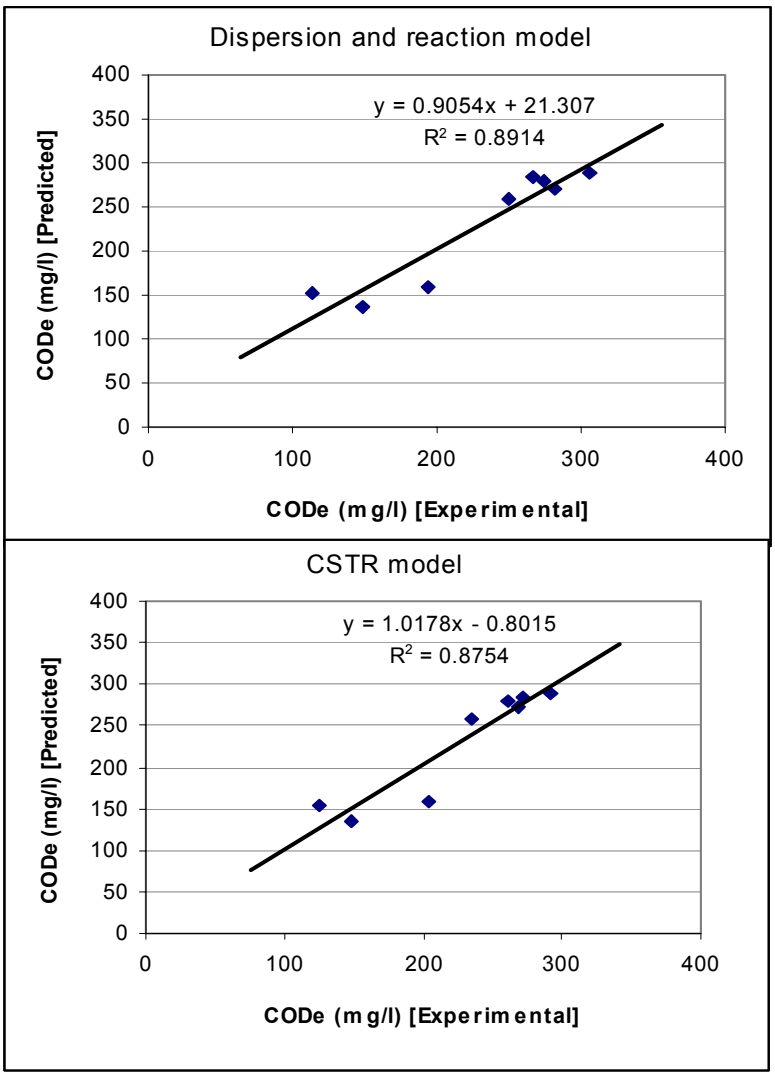

Figure 5.10 Experimental and predicted values of COD_t.

$$\frac{S_e}{S_o} = \frac{4ae^{1/2\delta}}{(1+a)^2 e^{a/2\delta} - (1-a)^2 e^{-a/2\delta}} \qquad (5.5)$$

$$a = \sqrt{1+4k\theta.\delta} = \sqrt{1+0.69\theta\delta}$$

$$S_e = \frac{S_o}{1 + 0.228\theta} \tag{5.6}$$

Figure 5.10 shows that the dispersion and reaction model predicted the effluent COD_t concentration more closely than the CSTR model. Although the difference in the correlation coefficients is very small, it is worth noting that the *k* value for the dispersion and reaction model has a smaller standard deviation than the corresponding *k* value for the CSTR model. Furthermore, Equation 5.5 is a general model that holds well over a wide range of dispersed flow patterns varying from plug flow to complete mixing (Levenspiel, 1999). In contrast, Equation 5.6 is only true for completely mixed reactors, which are not always found in real situations. For instance, the UASB studied herein showed a distorted mixed flow pattern at the beginning and towards the end of the evaluation period. This distortion affects the degree of conversion and hence the kinetics of the anaerobic treatment process. Thus, the variation of *k* obtained with the CSTR model may be due to the varying hydrodynamic conditions that did not conform satisfactorily to the underlying assumptions of the model.

In order to make use of Equation 5.5 for design purposes it would be necessary to have an independent expression to calculate δ values. Once δ is known together with *k* and the desired θ values, it would be possible to work out the effluent substrate concentration or removal efficiency of the reactor.

In an attempt to find such equation, multiple linear correlations were performed between *k*, δ, 1/δ and V_{up} values obtained from this study. Nonetheless, the correlation coefficients between different combinations of these variables were always low ($R^2 <$ 0.50). The latter clearly shows the necessity of more work on the hydrodynamics of high-rate anaerobic reactors in order to develop a sound approach to its design that takes into account not only biological aspects but also the interrelated hydrodynamic phenomena that occur in these complex biosystems. It is also desirable to carry out more hydrodynamic studies on full-scale reactors under real operating conditions since results from bench-scale or even pilot systems may not be reproducible at full-scale.

Details of the statistical analyses carried out in this Section are given in Appendix II in the file FULL-SCALE-EXP\UASB-TRACER-DISPERSION\ Removals.xls.

5.2 Pilot-scale experiments

5.2.1 Hydrodynamic studies on the pilot-scale APs

Hydrodynamic behaviour. Several authors have pointed out the inherent difficulties in accurately determining the mixing characteristics of bioreactors. Poor mixing is probably one of the main causes of faulty process performance (Bailey and Ollis, 1986; Levenspiel, 1999). Classical low-rate anaerobic reactors (e.g. septic tanks and anaerobic ponds) depend primarily on sedimentation and anaerobic digestion of the settled biosolids; thus, the driving forces for mixing are advection (water movement) and biogas bubbling up from the reactor sludge layer. Since the wastewater in these reactors merely flows over the sludge layer, mixing and contact are far from optimal. This explains the longer HRT values required for treatment in these systems.

On the other hand, high rate anaerobic reactors achieve at least the same efficiencies of low-rate reactors, but at much lower HRT values. This is because controlled intense mixing is promoted within the reactor volume by using advection (water movement) and biogas bubbling more efficiently. Another important factor in a high-rate reactor performance is the separation of biomass retention time from liquid residence time or HRT. The latter feature is normally uncontrolled in low-rate reactors. Thus, the modified configurations of AP evaluated in this study were intended to induce more efficient mixing due primarily to advection since the biosolids contents was low (5-8 percent of total volume), as was biogas bubbling, in all the pilot-scale AP.

The mechanisms promoting mixing in the different AP configurations are related to the water movement throughout the reactor. The average flow velocity in the baffled ponds (VBAP and HBAP) is higher and more controlled in each compartment (smaller cross-sectional area for the same flow rate in each compartment) compared to the average velocity in a similarly sized conventional AP. This result was found at the simulated baffled configurations discussed in Section 5.1.2. Furthermore, the changes in flow direction at the turning points may generate back mixing and consequently enhance contact. This is one of the main mixing mechanisms found in anaerobic baffled reactors (Barber and Stuckey, 1999). The two cross-sectional plastic screens provided in the PNFAP, are expected to function hydraulically as a flow distributor. Thus, preferential flow paths may be reduced and a more even flow field achieved. The MPAP has a reaction zone (mixing chamber) where the raw wastewater gets in contact with biomass aggregates via upflow velocity and biogas bubbling. The retention of

biomass is accomplished in the quiescent zone for settling provided in the horizontal flow compartment.

The RTD curves from Experiment I given in Figures 4.40 and 4.41 show a general trend in all AP towards a complete mixing pattern for all flow rates applied. However, the conventional pond (AP) always had a degree of short-circuiting since the peak values were higher than the expected theoretical figure (E_{max} = 1.0). The peak value at Q = 1.0 l/s was particularly high (E_{peak} = 2.75). This flow deviation, together with a dead zone volume, was also seen from the even higher values of E for $t/HRTt >$ 2.0 that produced a long RTD tail. The PNFAP showed a more stable behaviour as shown by its peak values (E_{max} from 1.0 to 1.2) and RTD shape. The BVAP had a slightly more unstable behaviour than the PNFP during the experiment. The δ values in Table 4.21 exhibit smaller variations for the PNFP, followed by the VBAP and then the AP. It is worth noting that maximum variations in δ values for these ponds were 20, 59 and 116 percent, respectively. The variances (σ^2 values) of the RTD curves also showed smaller variations for the PNFP and VBAP, compared to the AP.

The two-way ANOVA and Tukey multiple comparison tests run on the whole COD, TSS and Settleable solids effluent data sets showed a significant influence of the mixing configuration (i.e. VBAP, PNFAP and AP) and flow rates on the removal efficiencies of the units. The F-statistic test also confirmed a strong interaction between mixing configuration and flow rates. Thus, the null hypothesis was rejected, which means that there was a significant influence of the two factors on the performance of the APs evaluated at a 95% confidence level. It was also found that there was no significant statistical difference between VBAP and PNFAP for COD effluent concentrations. However, TSS effluent concentrations were slightly lower in the PNFAP configuration.

The results from Experiment II showed more variations in the RTD curves as shown in Figures 4.42 and 4.43. All AP configurations had some degree of short-circuiting, as the E_{peak} values were always higher than the maximum theoretical figure (E_{max} = 1.0). The conventional AP again registered the highest peak values, with a sharp early peak (E_{peak} = 2.52) for the last run (Q = 2.0 l/s). This early peak clearly indicates short-circuiting from inlet to outlet as described by Levenspiel (1999). Peña *et al.* (2000) found a similar RTD curve in a conventional full-scale AP treating domestic wastewater, which had been badly designed with the inlet and outlet being in adjacent (rather than diagonally opposite) corners. Figures 4.42 and 4.43 also show a prevailing long tail in the 2nd and 3rd runs (Q = 1.2 and 1.5 l/s) for the MPAP. However, this pond configuration dramatically improved its response in the last run (Q = 2.0 l/s) since the

RTD curve looked very close to the theoretical RTD for a tank in series model with two mixed reactors in series (Bailey and Ollis, 1986). Interestingly, this feature has been observed in high rate anaerobic reactors (UASBs) as reported by Bolle *et al.* (1985) and more recently by Avella (2001).

In this experiment maximum variations in δ values were 13, 31 and 54 percent in the MPAP, HBAP and AP, respectively. These figures confirm the high level of stability of the MPAP throughout the experiment, followed by the HBAP and then the AP. The improved hydrodynamic behaviour of the pilot-scale HBAP confirmed experimentally the results presented earlier on the CFD simulation of different baffled AP configurations at full-scale.

The two-way ANOVA and Tukey multiple comparison tests for COD, TSS and Settleable solids effluent data sets in this experiment again confirmed a significant influence of the mixing configuration and flow rates on the removal efficiencies of the APs. The F-statistic test also confirmed a strong interaction between mixing configuration and flow rates. Consequently, there was a significant influence of the two factors on the performance of the APs evaluated at a 95% confidence level. Contrary to results from Experiment I, all the configurations in Experiment II were statistically different in terms of both COD and TSS effluent concentrations.

The experimental results, together with the statistical analyses, showed that VBAP (operating at 1.5 and 1.9 l/s), PNFAP (operating at 1.5 l/s), MPAP (operating at 2.0 l/s) and HBAP (operating at 1.5 l/s) were the best ponds in terms of removal efficiency. They also exhibited a more stable hydrodynamic behaviour when compared to the control units (conventional APs) based on δ and σ^2 values. Another interesting feature is that the HRTe values for these ponds were 85 - 95 percent of the HRTt values, and this is a property of well-mixed reactors (Levenspiel, 1999).

Table 5.10 summarises the mass balances carried out on effluent (*C, t*) data sets to calculate the recovery of $[Li^+]$ at each AP and for every tracer test. In most cases the recovery of tracer was satisfactory and this showed that there were no problems of Li^+ attachment onto solids. The low dosage of Li^+ ($C_o < 0.60$ mg/l) also prevented likely toxicity problems for the biological process as recommended by Anderson *et al.* (1991).

Table 5.11 shows the retention factor ($\beta = Te/HRT_t$), total (V_t), active (V_a), and dead (V_d) volumes calculated at each AP configuration based on the hydrodynamic parameters presented in Tables 4.20 and 4.21.

Table 5.10 Summary of [Li^+] recovered at each tracer test in percentage.

Experiment	Pond	Run			
		1	2	3	4
I	VBAP	97	94	93	89
	PNFAP	90	71	94	97
	AP	90	92	90	89
II	HBAP	95	91	96	95
	MPAP	92	93	95	94
	AP	87	97	94	70

The weight of [Li^+] added in all the runs was 43 g (i.e. 261 g LiCl).

Table 5.11 Estimates of active and dead volumes in the pilot-scale AP.

Configuration		Experiment I			
		Q_d = 1.0 l/s	Q_d = 1.2 l/s	Q_d = 1.5 l/s	Q_d = 2.0 l/s
VBAP (V_t = 88 m^3)	β	0.88	0.90	0.88	1.00
	V_a	77	79	77	88
	V_d	11	9	11	0
PNFAP (V_t = 91 m^3)	β	0.92	0.86	0.88	0.83
	V_a	84	78	80	75
	V_d	7	13	11	16
AP (V_t = 82 m^3)	β	0.87	1.00	1.00	1.09
	V_a	71	82	82	89
	V_d	11	0	0	-7
		Experiment II			
HBAP (V_t = 88 m^3)	β	0.88	1.00	0.81	0.92
	V_a	77	88	71	81
	V_d	11	0	17	7
MPAP (V_t = 104 m^3)	β	0.79	0.92	0.89	1.00
	V_a	82	96	93	104
	V_d	22	8	11	0
AP (V_t = 82 m^3)	β	0.91	0.89	0.87	0.73
	V_a	75	73	71	60
	V_d	7	9	11	22

$V_a = T_e$ x Q or V_t x β; $V_d = V_t - V_a$; all volumes are expressed in m^3.
Q_d = Flow rate defined in the experimental design. The hydraulic loading rates applied to the AP varied slightly as shown in Table 4.20.

The β values obtained in experiment I tended to increase as the HRT decreased (i.e. increasing hydraulic loading rates) in the case of VBAP and AP. However, β decreased with decreasing HRT in the case of the PNFAP. It would seem that the AP had a better hydrodynamic performance since V_d was zero for Q_d values of 1.2 and 1.5 l/s. Nonetheless, the negative value of V_d obtained for the last hydraulic loading rate (Q = 2.0 l/s) at the AP indicates the same flow distortion identified in the UASB reactor.

This means that the first momentum (centroid) of the RTD is shifted towards the right of the expected theoretical value ($\theta = 1$) as a consequence of the curve's shape (i.e. descending branch above the theoretical CSTR curve). Thus, bypass flow coexisting with a mixed volume may yield a slightly higher value than the theoretical figure of $\theta = 1$ as discussed earlier.

It is worth noting that all the AP evaluated in both experiments received hydraulic and organic loading rates well above the maximum values currently recommended in the literature for conventional AP (Mara *et al*., 1992; Mara *et al*., 2001). RTD curves in Figures 4.40 and 4.41 together with hydrodynamic parameters in Tables 4.21 and 5.11 confirm that a mixed volume together with a dead zone can describe the overall mixing pattern in the VBAP and PNFAP. The degree of short-circuiting and bypass flows in these configurations was lower than in the AP. In general, the AP was less stable than the modified configurations despite that the physical design of this unit followed the recommendations for optimal performance given by Mara *et al.* (1992).

On the other hand, during experiment II the values of β showed a very slight increase for the HBAP as the hydraulic loading rate increased. This trend was similar to that of the VBAP during experiment I. The MPAP, however, showed a steady increase of β for successive increments in the hydraulic loading rate. Hence, the dead volume zone was steadily reduced as the mixing intensity increased. The combined flow direction within this AP (i.e. upflow in the mixing chamber and horizontal in the settling compartment) seemed to have no negative effects on its overall hydrodynamic pattern. It may instead be hypothesised that the two compartments may have influenced the response for the two-tank-in-series-like pattern. This fact provides reasons to believe that this configuration may achieve higher removal efficiencies than the others under steady state conditions.

The AP showed a steady reduction in β values during experiment II. Thus, the fraction of dead volume increased with the reduction of HRT, that is, as the hydraulic loading rate increased. Figures 4.42 and 4.43 together with hydrodynamic parameters in Tables 4.21 and 5.11 confirm that the AP configurations tested in experiment II can be described by a complete mixed model with coexisting dead volumes. Nonetheless, the dead volume incidence is higher in the AP, followed by the HBAP. In contrast, the MPAP tended to achieve CSTR behaviour as the hydraulic loading rate increased. Some degree of short-circuiting was also present, although its intensity was rather low given

the magnitude of E_{peak} values. The AP, however, showed a considerable intense short-circuiting from inlet to outlet during the maximum hydraulic loading rate test.

The results obtained in this experiment show major differences with results presented earlier on both full-scale reactors (AP and UASB). The hydrodynamic behaviour of the modified pilot-scale AP showed a global improvement compared to the conventional AP run as control for both experiments. Additionally, the modified configurations did not show extreme flow pattern distortions as those found in the full-scale reactors, particularly in the AP. The closeness to the CSTR pattern in the baffled configurations (VBAP and HBAP) and the MPAP, suggest a potential to handle higher organic loads at lower HRT since an improved mixing may overcome the inefficiencies found in the full-scale AP studies.

The CFD modelling results obtained for the full-scale AP showed that baffling arrangements have the potential to improve significantly the hydrodynamics of the pond. This result was confirmed with the pilot-scale baffled configurations. On the other hand, the MPAP was designed like a hybrid system between a conventional AP and a UASB reactor. This modified AP configuration seemed to converge to a CSTR model with increments in the hydraulic loading rate. This same result was observed and discussed earlier in the hydrodynamic study of the UASB reactor. Hence, it would seem that one of the prime prerequisites for the high-rate AP concept, that is, enhanced mixing, has been achieved by introducing simple changes into the classical physical design of anaerobic ponds.

At this point it is worth noting again that the sludge contents was deliberately kept low during the hydrodynamic evaluation of the pilot-scale AP. The whole idea was to know first the hydrodynamic behaviour due to the interaction between the water movement (advection) and the modified configurations. Once this variable was studied then a process performance evaluation would complete the picture by including the sludge effects. Based on the results from full-scale experiments and data reported in the literature, it is known that an appropriate amount of sludge within the AP enhances mixing and contact which in turn improves process performance. Azbar *et al.* (2001), pointed out that reactor configuration and substrate complexity influence the performance of anaerobic treatment processes. Their specific results may not be directly applicable since they worked on bench-scale reactors; however, the fact that CSTR configurations either in two-phase or single stage (i.e. UASB) yielded the best removal efficiencies, provides good evidence to pursue this flow pattern in the development of the high-rate AP concept. The other two features of a high-rate reactor, that is, the

biomass retention capacity and the separation of the sludge residence time from the HRT will be discussed in the Section dealing with process performance under steady-state conditions.

Process performance. Table 4.18 gives the pH and temperature ranges of the raw wastewater and effluents of the APs. These two parameters varied consistently in the influent during both experiments. The influent temperature range was 23 – 26 °C, and the pH varied from 6.3 to 7.4. Temperature values in the effluents ranged from 23 to 27 °C and pH varied from 6.0 to 6.8. The small pH reduction observed in the APs effluent is normal for anaerobic reactors treating domestic wastewater.

On the other hand, the hydraulic loading rates applied during the experiments were fairly stable since *CV* values were always below 0.10 as shown in Table 4.19. This same trend was observed in the physicochemical parameters of the influent as displayed in Table 4.22.

The volumetric organic loading rates (λ_v) applied to the APs are given in Table 4.20. The lowest λ_v applied was 372 g COD/m^3 d, whilst the highest was 1394 g COD/m^3 d. These values were for a HRT_t of 1.0 and 0.46 d, respectively. Current guidelines given by Mara *et al.* (1992) recommend a design limit for λ_v of 300 g BOD_5/m^3 d, which in terms of COD for a typical domestic wastewater is around 600 g COD/m^3 d. This value is recommended for temperatures above 20 °C and a minimum HRT of 1.0 d. Hence, the APs were loaded according to the design recommendations only for the flow of 1.0 l/s. At higher flows the APs were loaded up to 2.3 times the λ_v design value.

The removal efficiencies obtained during both experiments were most probably below the maximum attainable since the APs were seeded with minimal sludge contents as described in Sections 3.3.5 and 4.2.1. Consequently, the effluent concentrations and removal efficiencies of COD, TSS and settleable solids plotted in Figures 4.44 and 4.45 are only gross indicators of the treatment potential in the pilot-scale APs. The main purpose of these parameters was to confirm statistically the likely differences in removal efficiencies related to the combined effect of pond configuration and hydraulic loading rate variation.

The average COD effluent concentration in Experiment I had similar values in all the ponds for the first three hydraulic loading rates (1.0, 1.2 and 1.5 l/s). For the maximum hydraulic loading rate, however, the VBAP produced the lowest average COD effluent concentration, followed by the PNFAP and then the AP. The highest

average COD removal during the experiment was achieved by the PNFAP with 63% for an HRT_e of 0.62 d (Q = 1.5 l/s).

Average effluent TSS concentrations were very similar in all the APs. However, the best average TSS removal was achieved by the PNFAP with 71%, followed by the VBAP and then the AP, with average values of 65 and 60%, respectively.

Average settleable solids removals were always high in all the APs and seemed to be unrelated to the hydraulic loading rates applied. Nonetheless, the VBAP had the best efficiency (81%), followed by the PNFAP and the AP, both with 78%.

The removal efficiencies during Experiment II were a little lower compared with the values obtained in Experiment I. Average COD effluent concentrations and removals showed a very close variation in the three APs as shown in Figure 4.45. The MPAP, however, displayed an increasing efficiency with increasing hydraulic loading rates. The other two AP showed a more scattered response in COD removal efficiency as the hydraulic loading rate increased.

Average effluent TSS concentrations were lower during this experiment compared to Experiment I. The most stable pattern was shown by the MPAP with TSS removal efficiencies varying from 63 to 70%. The HBAP removed between 54 and 75% of the influent TSS throughout the experiment. The AP yielded the lowest removal efficiencies, 63 to 68%.

Average settleable solids removals were exceptionally good throughout the experiment in all the APs; however, they decreased with increasing hydraulic loading rates. The best removals for this parameter were obtained in the HBAP (76 – 96%), followed by the MPAP (82 – 95%) and then the AP (85 – 91%). Recent work reported by Mara *et al.* (2001) found that two overloaded conventional pilot-scale AP receiving domestic sewage (λ_v = 413 g BOD_5 /m^3 d) were able to remove only between 44 to 59% of the influent BOD_5 concentration.

The COD and TSS removal efficiencies found in this part of the research compare well with the removal efficiencies found for the same parameters in the full-scale studies carried out on the AP and the UASB at Ginebra. This result is important taking into account that the full-scale reactors and the pilot-scale AP all received the same wastewater under the same environmental conditions. In consequence, the treatment potential of the modified AP seems promising if one considers that process performance results (i.e. COD, TSS and settleable solids removals) obtained in this experiment may correspond to a pseudo steady-state condition of the biological process.

It may be hypothesised that once the best modified AP configurations reach steady-state conditions, their removal efficiencies could improve substantially.

Statistical correlations. Multiple linear regressions by least squares method were performed on the data shown in Tables 4.20 and 4.21, and the data series given in Appendix II in the file PILOT-SCALE-EXP\EXPERIMENT-II. Table 5.12 summarises the statistically significant regression models found for each AP.

Table 5.12 Summary of statistically significant regression models for each AP.

AP configuration	Parameter	
	COD	**TSS**
VBAP	$\frac{S_e}{S_i} = \frac{1.443}{\theta} + 0.201Pe - 0.137$	$TSS_e = 153.668 - 0.203TSS_i - \frac{170.663}{\theta}$
	Multiple R = 0.94, R^2 = 0.90	Multiple R = 0.98, R^2 = 0.97
PNFAP	$\frac{S_e}{S_i} = \frac{4.656}{\theta} + 0.273Pe - 0.564$	$TSS_e = 109.9 - 0.129TSS_i + \frac{102.1}{\theta}$
	Multiple R = 0.93, R^2 = 0.87	Multiple R = 0.51, R^2 = 0.26*
AP	$\frac{S_e}{S_i} = \frac{25.629}{\theta} + 0.912Pe - 2.639$	$TSS_e = 85.165 - 0.049TSS_i + \frac{392.288}{\theta}$
	Multiple R = 0.99, R^2 = 0.98	Multiple R = 0.88, R^2 = 0.77
HBAP	$\frac{S_e}{S_i} = \frac{1.687}{\theta} - 0.204Pe + 1.037$	$TSS_e = 32.801 + 0.128TSS_i + \frac{144.62}{\theta}$
	Multiple R = 0.87, R^2 = 0.76	Multiple R = 0.60, R^2 = 0.36*
MPAP	$\frac{S_e}{S_i} = -\frac{3.619}{\theta} + 0.026Pe + 0.661$	$TSS_e = \frac{398.311}{\theta} + 0.234TSS_i - 2.297$
	Multiple R = 0.88, R^2 = 0.78	Multiple R = 0.95, R^2 = 0.90
AP	$\frac{S_e}{S_i} = -\frac{1.477}{\theta} - 0.027Pe + 0.69$	$TSS_e = \frac{89.59}{\theta} + 0.233TSS_i + 14.898$
	Multiple R = 0.91, R^2 = 0.83	Multiple R = 0.91, R^2 = 0.83

Subscripts: e, effluent (mg/l); i, influent (mg/l) θ = HRT (h)
* Regression models with very poor correlation

The linear regression models in Table 5.12 display a similar form to the CSTR model with first-order kinetics (Equation 2.40). COD effluent concentration is a function of 1/θ in all these expressions. The same type of model was also obtained for TSS removal. The second term in the COD regression models takes into account the mixing and dispersion factors since the Peclet number (Pe = 1/δ) is a dimensionless group that quantifies these phenomena (Bailey and Ollis, 1986). Most of the correlations yielded an adequate fit between the experimental data with the exception of TSS correlations for the PNFAP and the HBAP. The statistical correlation parameters

show the adequacy of each regression model and suggest that a CSTR was the underlying hydrodynamic pattern in the pilot-scale APs.

The hydrodynamic improvements (i.e. better mixing pattern) observed in the modified APs give reason to believe that the biological process performance may also be enhanced. In this sense, Bailey and Ollis (1986) highlight the importance of adequate flow mixing and transport phenomena since both of these factors greatly affect the kinetic behaviour of microbial cells. These authors argue that turbulent mixing caused by velocity fluctuations has important implications on the metabolic state of microorganisms at different time and space scales. In agitated bioreactors, for instance, the smallest eddy size may be of the order of 20-100 μm. At such a scale, bioflocs of microorganisms and diverse cell aggregates may be substantially influenced by velocity and mixing intensity fluctuations. Heavy distortions of these factors may cause a transient metabolic state in the cells that will lead to substrate conversion inefficiencies at the macro level. Therefore, an even mixing pattern at the macro level is desirable so as to provide good conditions for substrate transport to and from the microbial aggregates. Although this work did not study these phenomena at the micro scale, it is important to recognize their effects and interconnections with the overall hydrodynamic behaviour of a given reactor.

Based on the data gathered in this experiment, it seems possible to increase the applied volumetric organic loading rate in the modified AP configurations up to 0.8–1.0 kg COD/m^3 d, with a subsequent reduction of HRT_t to 0.5 days, for temperatures around 23°C.

The results also indicate that further work on the development of the high-rate anaerobic pond concept based on improved hydrodynamics should be done to investigate more AP configurations. This is important since, as pointed out by Mulder *et al.* (2001), efficient reactor hydrodynamics is a crucial factor to achieve the highest conversion capacity by using the available biomass in the system in the best way possible.

5.2.2 Process performance of the pilot-scale APs

As mentioned earlier, two out of the four AP configurations evaluated in the hydrodynamic study were monitored for an additional 5-month period in order to study the biological process performance under steady-state conditions. The APs were studied under three different hydraulic loading rates. The conventional AP was run again as the

control unit for the whole experiment. The evaluation of steady-state performance was carried out in three periods of six weeks each. A transitional period of two weeks was left between successive hydraulic loading increases so as to reach a new steady-state. The latter was judged as achieved once the differences in removal efficiencies for COD_t, TSS and settleable solids were less than 10% in at least three consecutive daily grab samples taken within the two weeks transitional period.

Flow, pH and temperature. Hydraulic loading rates were rigorously controlled during the monitoring period. The *CV* values in Table 4.24 show the low variation in the applied hydraulic loading rates to all APs. The MPAP received slightly higher loading rates given its bigger volume compared with the other two APs. The theoretical HRT varied from 26 to 12 h in all APs. Hence, they were loaded as recommended in the current literature at the beginning of the monitoring period, but towards the end of the study they received about twice the maximum current design load.

The temperature of the raw wastewater varied from 23.1 to 28.6 °C, and the AP effluents had slightly higher maximum temperatures at around 29.6 °C. The raw wastewater had pH values around neutrality. The slightly lower pH values recorded in the AP effluents were typical of anaerobic reactors for the treatment of domestic wastewater. In all cases effluent pH values were above 6.2. This confirmed that there was no risk of acidification in any of the AP throughout the monitoring period (this aspect is further discussed below together with other parameters).

The composition of the raw wastewater remained relatively constant during the five-month period as shown by the data in Table 4.26 and their respective descriptive statistics. The relatively long distances (i.e. travel time) of the sewerage network together with the high temperatures recorded during the period may explain the presence of a small concentration of VFA in the influent. This feature has been reported in other studies carried out at the site (Jacome and Marin, 2001). The alkalinity concentration of the influent was high enough to apply anaerobic treatment safely. The average ratio of COD_t to COD_f ($COD_t/COD_f = 3.4$) showed a high content of particulate material in the raw wastewater during the period of study.

Organic matter removal. Unlike the previous experiment, data from this stage showed a definite improvement in organic mater removal in the modified AP (MPAP and HBAP). The removal efficiency of the conventional AP was always lower than those of the APs with modified configurations.

Figure 4.46 shows that the MPAP steadily improved its removal efficiency for both COD_t and COD_f as the hydraulic and organic loading rates increased. Average

removal efficiencies of COD_t ranged from 77 to 79% during the monitoring period. The average COD_f removal efficiency also increased, from 50 to 78%, and this is a remarkable improvement that demonstrates the large participation of biological activity in the overall removal of organic matter.

The HBAP achieved lower COD removal efficiencies for both COD_t (65-51%) and COD_f (41-44%). The best operating point for this AP was at a HRT of 18 h with removal efficiencies of 67 and 51% for COD_t and COD_f, respectively.

In contrast, the conventional AP showed a continuous deterioration of the effluent quality after the first stage (i.e. HRT < 24 h). Average COD_t removal efficiencies varied from 67 to 49%; and COD_f removals ranged from 44 to 53%, although an average COD_f removal of only 28% was recorded during the second stage (i.e. HRT = 18 h) for this AP. The poor performance of the conventional AP (in terms of COD removal) found in this study confirmed the adequacy of the maximum volumetric organic load criterion to the design of conventional low-rate AP as recommended by Mara *et al.* (1992). Table 5.13 displays the average COD_t and COD_f removal efficiencies together with the maximum attainable COD removal efficiency based on filtered effluent samples.

Table 5.13 Summary of average COD removal efficiencies (%) in the APs.

Configuration		Stage 1			Stage 2			Stage 3		
		COD_t	COD_f	COD_m	COD_t	COD_f	COD_m	COD_t	COD_f	COD_m
HBAP	Mean	65	41	85	67	51	88	51	44	81
	σ	4.7	24.3	3.3	6.4	19.3	4.5	8.2	11.6	4.2
	CV	0.07	0.59	0.04	0.10	0.37	0.05	0.16	0.26	0.05
MPAP	Mean	77	50	88	78	75	93	79	78	93
	σ	4.1	31.0	5.5	8.7	11.4	2.9	3.7	7.0	1.6
	CV	0.05	0.62	0.06	0.11	0.15	0.03	0.05	0.09	0.02
AP	Mean	67	44	85	48	28	83	49	53	84
	σ	3.1	19.1	5.0	12.8	48.9	8.9	15.0	21.7	7.1
	CV	0.05	0.43	0.06	0.27	1.75	0.11	0.30	0.41	0.08

t, total; f, filtered; m, maximum

Table 5.13 show the differences in organic matter removals (measured as COD) within and between the AP. It is worth noting that the smallest differences between CODt and CODmax removals were obtained in the MPAP, followed by the HBAP, and then the AP.

Figure 4.47 shows the performance of the APs with regards to TSS and VSS effluent concentrations and removals. Both of these parameters showed exactly the

same trend in all three AP. Parallel lines for TSS removal efficiencies were obtained with the highest figures occurring in the MPAP (71-76%), followed by the HBAP (64-73%), and then the AP (51-59%). The VSS removals followed the same trend with the following figures: MPAP (66-82%), HBAP (58-81%) and AP (46-74%). The lowest TSS and VSS removal values were obtained for the highest hydraulic loading rate applied of 2.0 l/s (HRT = 12 h).

The rate of VSS lost in the effluent was higher than that of the TSS in all three APs as shown in Figure 4.47. This effect contributed to the reduction of COD_t removal particularly in the HBAP and the AP. The higher removal of COD_f in the MPAP counterbalanced the negative effect of effluent TSS and VSS contents and this explains why COD_t removal in this configuration was able to increase steadily during the study.

Apart from the increase in CODt effluent concentration, the loss of VSS can be directly related to the washout of active biomass. This effect has negative implications on process performance since the reactors will experience a reduction of their treatment capacity. This same negative effect has been reported in the literature for UASB and ABR reactors (van Haandel and Lettinga, 1994; Grobicki and Stuckey, 1991; Barber and Stuckey, 1999). The control of biomass washout is directly related to the sludge retention in the reactor, and this is discussed in more detail below.

Environmental conditions. The healthy development of the anaerobic treatment process in the APs was monitored through VFA, SO_4^{2-}, alkalinity and ORP. These parameters were measured in the influent and effluent of the APs throughout the study.

VFA effluent concentrations ranged from 3.3 to 3.9 meq/l at the beginning of the first stage whereas the influent concentration was 2.8 meq/l. The concentrations of VFA were lower and more stable after the second week and from there on they remained below 2.0 and 3.0 meq/l in the influent and effluents, respectively.

On the other hand, alkalinity showed a stable behaviour in the influent and all the effluents during the study. Figure 4.51 shows the variation of this parameter, which increased in the effluents during the last stage. Table 5.14 shows the average values of VFA, alkalinity and SO_4^{2-} per stage.

The low effluent concentrations of VFA together with the positive variation of alkalinity and the stable pH values confirmed that there was no risk of process acidification at any stage. Alkalinity concentration showed a net increase in all AP effluents during the study as shown in Table 5.14. This is a characteristic of well functioning anaerobic reactors for sewage treatment due to ammonification of proteins and VFA degradation (Rodriguez *et al.,* 2001; van Haandel and Lettinga, 1994).

Table 5.14 Average effluent concentrations of VFA, alkalinity and SO_4^{2-}.

Configuration		Stage 1			Stage 2			Stage 3		
		VFA	Alk.	SO_4^{2-}	VFA	Alk.	SO_4^{2-}	VFA	Alk.	SO_4^{2-}
HBAP	Mean	2.2	243	12.8	2.1	244	24.8	2.2	256	58.9
	σ	0.9	9.5	6.6	0.6	6.0	17.4	0.3	40.8	25.0
	CV	0.41	0.04	0.51	0.27	0.02	0.70	0.14	0.16	0.42
MPAP	Mean	2.1	259	13.0	1.9	260	11.2	1.7	265	27
	σ	0.7	11.0	16.6	0.7	13.9	10.9	0.5	37.6	14.4
	CV	0.36	0.04	1.27	0.36	0.05	0.97	0.28	0.14	0.53
AP	Mean	2.5	247	7.1	2.3	245	27.2	2.6	250	62.3
	σ	1.0	6.6	5.4	0.7	29.3	29.5	0.3	38.7	24.1
	CV	0.40	0.03	0.75	0.31	0.12	1.09	0.10	0.15	0.39

VFA in meq/l; alkalinity in mg $CaCO_3$/l and SO_4^{2-} in mg/l.

The ORP variations in Figure 4.52 displayed typical values for the influent and all the effluents. The raw wastewater had ORP values mostly on the positive side of the scale and just one sample had an ORP value below –50 mV. All the effluents had negative ORP values during the study, mostly in the range –125 –200 mV. These ORP values confirm the characteristic reducing power of anaerobic environments that prevailed throughout the monitoring period.

On the other hand, influent SO_4^{2-} concentration ranged from 60 to 100 mg/l but there were peak concentrations of up to 130-180 mg/l at each stage. The average COD/SO_4^{2-} ratio in the influent was 6.5. The peak influent SO_4^{2-} concentrations may cause transient problems of odour and also upset the methanogenic activity due to competition between SRB and AMB (Visser, 1995). However, for SO_4^{2-} concentrations less than 500 mg/l in the raw wastewater, there should be no problem with odour release in well-designed and operated AP (Mara *et al.,* 1992). Rinzema (1988) and Visser (1995) pointed out that at low sulphate concentrations (i.e. domestic wastewater), the growth of acetotrophic SRB is limited, and AMB will outcompete them. Consequently, at COD/SO_4^{2-} ratios normally encountered in domestic wastewater, acetotrophic methanogenesis will not be inhibited provided that the reactor is properly loaded. Nonetheless, the oxidation of hydrogen and propionate may be still carried out by SRB. Lin and Yang (1991) recommend a minimum COD/SO_4^{2-} ratio of 7 to 10 in the influent regardless of the pH value. This is a safe limit to avoid problems of odour, corrosion and toxicity. Choi and Rim (1991) reported that COD/SO_4^{2-} ratios above 2.7 would ensure the predominance of AMB. Van Haandel and Lettinga (1994) argue that sulphide concentrations of up to 50 mg/l normally expected in domestic wastewater treatment, are far lower than the minimum concentration needed to cause inhibition or toxicity.

Visser *et al.* (1996) found that at pH levels below 6.9 AMB will outcompete SRB, whereas at pH above 7.7, SRB will win the competition. These authors also found that methanogenic activity in dispersed-type sludge would be inhibited by 50% if the H_2S concentration exceeds 50 mg/l.

The effluent SO_4^{2-} concentrations were highly variable in the HBAP and the AP. The MPAP effluent had less variability in SO_4^{2-} concentration as shown in Figure 4.50. Interestingly, the highest effluent SO_4^{2-} concentrations found in the HBAP and the AP occurred in those samples with the higher contents of TSS collected during the last stage. This was not the case for the MPAP as can be seen in Figure 4.50. Average values in Table 5.14 demonstrate that the MPAP was better able to handle the SO_4^{2-} influent concentrations compared to the other two AP. The average effluent SO_4^{2-} concentrations reported in Table 5.14 compare well with data in Veenstra *et al.* (1995) on their evaluation of an AP in the Yemen Republic.

The experimental data together with the studies and findings quoted earlier suggest that SO_4^{2-} conversions did not affect process performance in the APs. Additionally, there was no evidence of odour problems and the effluent concentrations of H_2S presented in Table 4.28 fell within safe limits.

Sludge characteristics. The three APs were seeded only at the beginning of the hydrodynamic study (Experiment II) as explained in Section 3.3.5. Thereafter only the incoming solids settling and biomass growth contributed to the development of the sludge bed in all the APs. Table 5.15 shows the sludge heights measured at three different times within the APs.

Table 5.15 Sludge heights measured in the APs (m).

Date	HBAP			MPAP		AP	
	Comp. 1	Comp 2.	Comp. 3	Mix. pit	Settler	L/3	2L/3
08/01	0.14	0.12	0.05	0.55	0	0.12	0.10
10/01	0.20	0.09	0.07	0.67	0.03	0.15	0.07
12/01	0.22	0.10	0.08	0.95	0.03	0.16	0.06

Sludge aggregates moved downwater through the compartments in the HBAP. The sludge height increased in the mixing pit of the MPAP, but this may have been due to the combined effect of biomass growth, incoming solids accumulation and bed expansion caused by the rising upflow velocities in the mixing pit throughout the three stages (0.45, 0.61 and 0.94 m/h). The lower sludge height found in the settling zone of the MPAP suggests that biosolids retention in the mixing zone was fairly effective. On

the other hand, the settling pattern in the AP showed a steady accumulation in the first third of the pond but it was more random at the sampling point located in the last third. The latter confirmed the unpredictable pattern of sludge settling observed in conventional AP, since the aggregates seem to move about under the combined influence of water flow, biogas bubbling, sludge resuspension and even sliding in high accumulation zones (Peña *et al.* 2000; Nelson and Jimenez, 2000; Warren, 1998).

Figures 4.53 and 4.54 show the concentration of TS and VS in the sludge from each AP. A total of eight samples per sampling point were taken during a period of 20 weeks that comprised the three stages of the study. The concentration of both TS and VS in the HBAP was consistently higher in the sludge samples from the first compartment compared with the samples from the third compartment. Minimum and maximum concentrations of TS and VS during the whole period for the first and third compartments were (TS = 51-106 g/l; VS = 29-41 g/l) and (TS = 32-92 g/l; VS = 16-46 g/l), respectively. The relation VS/TS in the first compartment was very stable with an average value of 0.48 whereas for the third compartment it was more variable with an average of 0.42. The values of the VS/TS ratio suggest the presence of undigested organic matter in the sludge from the first compartment although the inert material fraction seems also important. The lower concentrations of TS and VS in samples from the third compartment showed a lower sludge quality. In other anaerobic reactors like the ABR, the lower quality particles of sludge are generally shifted towards the downstream compartments (Grobicki and Stuckey, 1991). These sludge particles may eventually leave the reactor with the effluent during transient flows or by biogas outbursts occurring near the outlet. The latter was frequently observed in the HBAP during the last stage of the study.

TS and VS concentrations in the mixing pit of the MPAP were more variable. Part of this variability, however, could be related to the sampling procedure since it was difficult sometimes to keep the peristaltic pump intake hose fixed at the same point. Minimum and maximum concentrations of TS and VS in the sludge from the mixing pit were 48-126 g/l and 23-80 g/l, respectively. Minimum and maximum TS and VS concentrations at the settling zone samples were 39-170 g/l and 20-81 g/l, respectively. The higher TS concentration found in the samples from the settler may be related to the likely compaction of the sludge in this zone. The ratio VS/TS in the mixing chamber was 0.50 on average. This value compares well with data from the UASB reactor at Pedregal, Brazil (VS/TS = 0.55) and the data presented earlier on the start-up of the UASB at Ginebra (VS/TS = 0.48). The VS/TS ratio in the settling compartment was

0.43 at the beginning of the evaluation period but it increased to 0.48 during the second and third stages.

Figure 4.54 shows that concentrations of TS and VS at the sludge layer in the conventional AP had a random pattern during the study. There was no clear trend for VS and TS values at any of the two sampling points. Minimum and maximum concentrations of TS and VS in the sludge from the first third of the AP were 24-109 g/l and 12-56 g/l, respectively. Likewise, minimum and maximum concentrations of TS and VS in samples from the last third of the AP were 36-86 g/l and 19-39 g/l, respectively. The ratio VS/TS in the first third of the AP was more variable compared to the last third. The ratio in the former varied from 0.46 to 0.57, which suggests an important contribution of fresh organic matter (VSS) to the ratio average value of 0.52. In contrast, this ratio was more constant in the sludge from the last third (0.44-0.50) of the AP. This lower average value of 0.48 also suggests a more stable sludge towards the downstream end of the AP. These results demonstrate the more unpredictable behaviour of the sludge layer in conventional AP. Similar results to these were found by Warren (1998) working on the sludge dynamics of a full-scale AP in Australia.

Considerations on biomass retention in the pilot-scale AP. The performance of high-rate anaerobic reactors depends on mixing intensity and contact pattern, biomass retention and the successful separation of cellular (sludge) residence time from liquid HRT. So far the mixing and contact pattern of the pilot-scale APs have been discussed in the preceding Sections. However, it is also important to determine the other two factors in order to check for the characteristic high-rate features in the modified APs proposed herein. First of all, it is important to recall that modern high-rate anaerobic reactors retain the anaerobic biomass by two main mechanisms: biofilm growth on support media (immobilised biomass) or physical liquid-solid separation of the active suspended biomass from the liquid phase. In the latter the biosolids are returned to the reaction zone after settling. Examples of the biofilm reactors are the anaerobic filters and the granular beds operated in either a fluidised or expanded mode (van Haandel and Lettinga, 1994). The UASB reactor is probably the most widespread anaerobic system - in the second category- for domestic wastewater treatment in the tropics, and it uses an in-built settler for biomass separation and retention.

The modified AP configurations evaluated in this study fall in the category of reactors with physical liquid-solid separation. The conventional AP relies basically on the efficiency of gravity settling to retain the active biomass. However, the full-scale studies presented earlier together with the CFD simulation results and previous work

reported in the literature, show that the settling efficiency in AP tends to decrease as operation time passes. Settled sludge is continually resuspended from the biosolids layer by biogas outbursts. This effect together with gradual sludge accumulation and flow distortions may induce a washout of active biomass and a loss of active volume in the long term (Warren, 1998; Peña *et al.,* 2000). Therefore, the efficiency of biomass retention in conventional AP seems rather limited and uncontrolled and this may explain its relatively low efficiencies compared to high-rate anaerobic reactors.

On the other hand, the CFD simulations showed that, apart from mixing the AP volume, baffling also redistributes more evenly the velocity field. Thus, baffling might improve sludge dynamics and its influence on treatment efficiency since a more controlled or predictable settling pattern might be expected as result. The experimental evidence obtained at the HBAP showed that removal of TSS and VSS was much better in this pond compared to the conventional AP. However, the removal efficiency of solids (TSS and VSS) in the HBAP diminished with increases in hydraulic loading rate and elapsed operating time. This demonstrates, together with the data in Table 5.15, that there was transport of biosolids from the first to the last compartment of the HBAP. Grobicki and Stuckey (1991) and Barber and Stuckey (1999) found a similar effect of biosolids transport from inlet to outlet with increasing hydraulic loading rate in an ABR. The biogas production also moved downstream in the HBAP since biogas outbursts causing biosolids loss in the effluent were observed close to the outlet during the last stage. It would seem that biomass retention efficiency in the HBAP is related to hydraulic loading rate, which in turn affects flow velocity at each compartment. Hence, the number of compartments in baffled AP seems to be the key variable to find the balance between biosolids transport rate and overall biomass retention efficiency in the system.

As mentioned earlier, the MPAP configuration had the best removal efficiencies of COD_t, COD_f, TSS and VSS for a HRT as low as 12 h. These high removal efficiencies are comparable to figures reported for high-rate anaerobic reactors treating domestic wastewater. Apart from the improved hydrodynamic behaviour (CSTR) found in the MPAP, it is believed that biomass retention and its concomitant sludge retention time played a significant role in the performance of this AP configuration.

The biomass retention in the MPAP relies on settling in the horizontal flow compartment once the influent flows out from the mixing chamber. However, it is believed that an additional mechanism of solids intersection and filtration occurring in the transition zone between the mixing chamber and the settler may have played a

central role in biomass retention. As explained in Section 3.2.2, the transition between the mixing chamber and the settler is done via a four-layered arrangement of plastic screens. Figure 5.11 shows the details of the plastic screens arrangement and a photograph of the biofilm growing on the screens during the study.

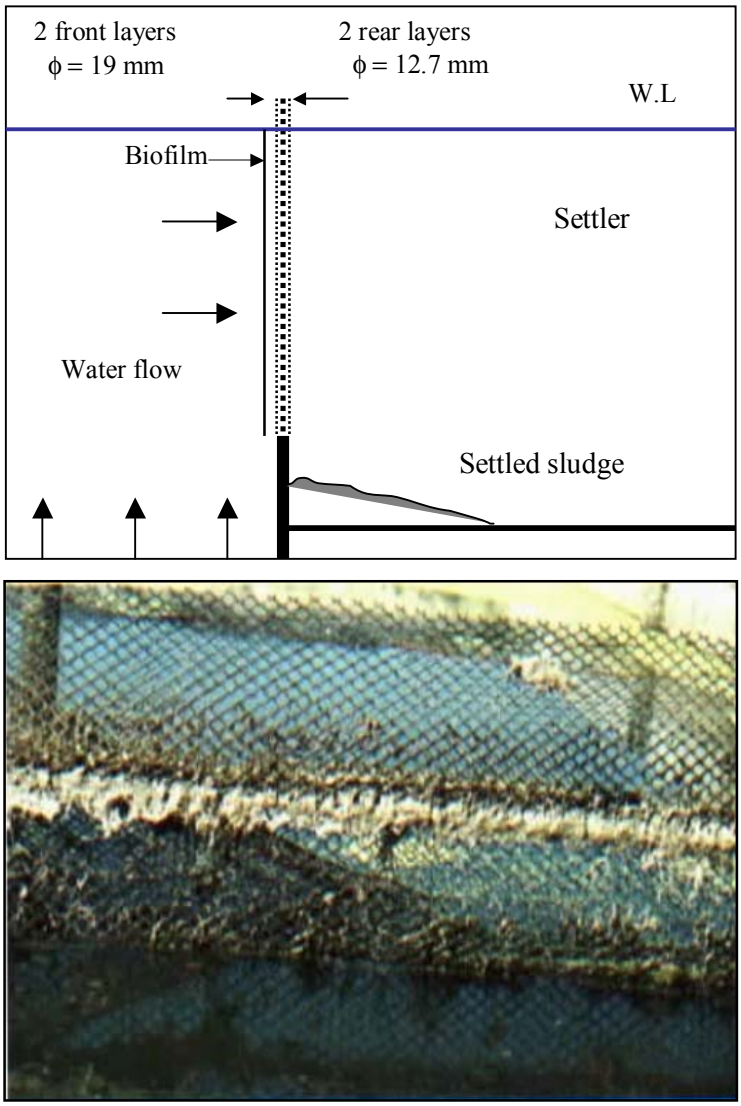

Figure 5.11 Biofilm growth in the transition zone (screens) in the MPAP.

Figure 5.11 shows the thick anaerobic biofilm that grew on the plastic screens that provide the transition between the mixing chamber and the horizontal settler compartment. It was observed that some fibres from the raw influent got trapped in the screens and served as additional support material for the biofilm. The photograph was taken some minutes after the water was drained down few centimetres in order to see the biofilm. However, once the biofilm was exposed to the air, it started to slough off the screens. The low sludge depth measured in the settler compartment (0.03 m) during the study suggests that biomass retention in the mixing chamber was efficient. Further

research, however, is needed to study the role of the screens and biofilm development on the intersection-filtration of biosolids and other likely biochemical conversion processes.

On the other hand, the transition zone (screens) together with the horizontal settling compartment of the MPAP seemed to be more efficient than the settling under vertical upflow direction in the UASB reactor. The best results in the latter were obtained during the steady-state period following the start-up phase with an average value of 71% TSS removal. Nonetheless, this efficiency fell to an average of 65% TSS removal during the hydrodynamic study of the reactor. In contrast, the MPAP had average TSS removals between 71 and 76% during the whole period of the process performance evaluation. The major differences between the UASB and the MPAP were basically the transition between the mixing chamber and the settling zone itself since the mixing chamber of the MPAP was designed by keeping hydraulic similarity with the UASB (i.e. same density of feeding points, 2.9 m^2/inlet point, and upflow velocities in the same range than those applied to the UASB during its hydrodynamic study). According to Narnoli and Mehrotra (1997), a typical sludge particle in the blanket of a UASB is under the combined action of three main forces: its own weight, the buoyant force induced by biogas bubbling and the resisting drag force. All these forces act in the vertical direction and the net movement of the particle will depend on its settling properties and its interaction with biogas bubbles. However, the liquid upflow velocity would cause a fourth force on the particle in the upward direction. Thus, the dynamic equilibrium in this situation will tend to move the sludge aggregates upwards (i.e. especially those particles with poor settling properties). The situation may be worse under transient hydraulic overloads that might cause a massive washout of biomass.

In contrast, the dynamic equilibrium in the settler of the MPAP will have only the drag force of the fluid acting in the horizontal direction combined with the particle weight for settling. The buoyancy force should be minimal, not to say zero, since the particle in the settler is out of the influence of biogas bubbling, which happens mostly, not to say exclusively, in the mixing chamber. Therefore, these subtle differences in the interaction between sludge aggregates, liquid and biogas help to explain the improved efficiency of organic matter removal together with the better biomass retention recorded in the MPAP. These characteristics together with the experimental results presented earlier provide the basis for the concept of high-rate anaerobic pond. Table 5.16 displays data for comparison between UASB reactors treating domestic wastewater and the improved AP configurations studied herein.

Table 5.16 Some of the results published on the performance of UASB reactors for domestic wastewater treatment.

Reference	Temp.	HRT	$COD_{t\text{-}inf}$	Removals (%)		
	°C	(h)	(mg/l)	COD_t	COD_{max}	TSS
Grin *et al.*(1983)	20	18.0	550	55-75	-	-
	20	24.0	500-550	-	70	-
	20	8.0	500	-	75	-
Lettinga *et al.*(1983)	15-19	8.0	500	40-55	65-80	-
	8-20	12.0	500	67	65-80	-
	8-20	12.0	300	-	50-60	-
Vieira (1984)	35	4.0	341	65	83	61
Schellinkhout *et al.*(1985)	24-26	4.0-8.0	267	-	83-85	70
	24-26	3.0-3.5	267	-	78-85	-
Vieira and Souza (1986)	20	4.0	424	60	82	69
	23	4.0	406	65	83	69
Man *et al.*(1986)	12-18	7.0-12.0	500-700	40-60	-	-
	7-8	9.0-14.0	500-700	45-65	-	-
Nobre and Guimaraes (1987)	24-26	10.0-18.0	660	73	85-91	-
Vieira (1988)	21-25	4.7	265	50	-	73
Schellinkhout *et al.*(1988)	23-24	5.2	430-520	66	-	69
Monroy *et al.*(1988)	12-18	18.0	465	65	-	73
Barbosa and Sant'ana (1989)	19-28	4.0	627	74	89	72
Van Haandel and Lettinga (1994)	25	17.0	799	75	85	68
	25	8.0	239	67	-	78
	20	6.0	458	70	-	79
Dean and Horan (1995)*	20-32	10.0	487	79	89	75
Hammad (1996)	20	3.0-8.0	317-549	49-66	-	50-76
Monroy *et al.* (2000)	20	6.0	458	70	-	-
	20	6.0	500	70	-	-
	15	8.0	300	70	-	-
Rodriguez *et al*. (2001)	24-27	8.0	520	68	83	69
UASB**	22-24	7.9	460	58	84	65
HBAP**	23-26	18.0	600	67	88	67
MPAP**	23-26	12.0	590	79	93	71
AP**	23-26	24.0	597	67	85	59

* These figures refer to a UASB treating a mixed domestic and industrial wastewater.
** Results from the work presented here.

Table 5.16 shows that removal efficiencies in the HBAP (HRT = 18 h) are comparable with few of the studies reported in the literature for UASB reactors. Nonetheless, the best results were obtained with the MPAP (HRT = 12 h), and its efficiencies were even higher than those reported on several studies of UASB reactors. Recently published results on the development of a new approach to WSP design reported by Mara *et al.* (2001) showed that conventional pilot-scale APs operated at a HRT of 12 h in tropical regions had poor performances with BOD_5 removal efficiencies

of only 44%, whereas COD_t removal was as low as 26%. Oliveira *et al.* (1996) reported average COD_t removal efficiencies of 64 and 54 % at HRT values of 1.5 and 1.0 d, in a conventional pilot-scale AP operated in tropical conditions at EXTRABES in northeast Brazil. Results reported in the literature on both UASB and conventional AP applied to domestic wastewater treatment support the improvements achieved in the modified AP configurations evaluated in this study. Based on the high removal efficiencies attained mainly in the MPAP, it seems that it is indeed feasible to develop further the concept of high-rate AP for the advanced primary treatment of domestic wastewater in tropical regions. In this sense, the biogas can easily be recovered from the high-rate AP due to its smaller surface area and the existence of a definite anaerobic reaction zone where most of the biogas is produced and can be collected from. The improved biomass retention (i.e. high sludge retention time) will also produce a mineralised sludge easy to treat and dispose of. Nonetheless, the latter aspects together with operational variables deserve further research.

Removal of microbiological indicators. The removal of microbiological indicators was generally low in the pilot-scale APs as shown in Table 4.29 and Figures 4.55 and 4.56. The removal of FC was slightly better in the MPAP compared to the other two AP. The highest FC removals occurred during the second stage (HRT = 18 h) in all the ponds and they were 82.4, 90.5 and 89.1% for the HBAP, the MPAP and the AP, respectively. These figures are in agreement with data reported by Dixo *et al.* (1995) who studied the microbiological quality of an UASB effluent post-treated in a facultative pond. The average FC removal in their UASB reactor was 80%.

The removal of *E. coli* was higher in the conventional AP in all the stages. The maximum average removals were 91, 81.4 and 65.9% for the AP, the MPAP and the HBAP, respectively. The maximum removals occurred in the first stage for the AP and the MPAP and in the second stage for the HBAP. These figures are similar to the average removal efficiency of around 80% for *E. coli* reported by van Haandel and Lettinga (1994) in the UASB reactor at Pedregal, Brazil.

On the other hand, the average removal efficiency of helminth eggs was always better in the MPAP compared to the other APs in all the stages. The highest average removal efficiencies of helminth eggs were 67, 60 and 53% for the MPAP followed by the HBAP and then the AP. The MPAP had its best removal efficiency at stage 3 (HRT = 12 h), whereas HBAP and AP yielded their best efficiencies during stage 1 (HRT = 24 h). Dixo *et al.* (1995) found an average removal of helminth eggs of 63% in a UASB reactor in northeast Brazil. Van Haandel and Lettinga (1994) reported an average

removal of 80% of the influent helminth eggs concentration in the UASB reactor at Pedregal, Brazil.

The helminth egg removal equation proposed by Ayres *et al.* (1992) for the design of WSP, was applied to the experimental data in Table 4.29. However, this equation underestimated the effluent concentration of helminth eggs for all the APs with the exception of the MPAP operating at HRT = 12 h. In this case, the predicted removal efficiency value was 68%, which is in agreement with the experimental value of 67%.

Anaerobic reactors are very efficient at removing organic matter whereas their removal efficiency of pathogens is generally low. Probably with the exception of *Vibrio cholerae* removed at in-pond sulphide concentrations ≥ 3 mg/l (Oragui *et al.* 1993) and the removal by settling of helminth eggs and the pathogenic protozoa *Giardia* spp. and *Cryptosporidium* spp. (Grimason *et al.*, 1993) in AP, there are very few other references in the literature regarding pathogen removal in anaerobic ponds treating domestic wastewater.

The efficiencies found in the high-rate AP configurations for FC, *E. coli* and helminth eggs conformed to removal values reported in the literature for anaerobic reactors. However, it seems possible to improve these efficiencies if biomass retention is further enhanced in the high-rate AP.

COD modelling and statistical correlations. Influent and effluent CODt and CODf data were applied to the CSTR model with first-order reaction (Levenspiel, 1999) and also to the dispersion model with first-order reaction kinetics proposed by Wehner and Wilhelm (1956). Table 5.17 summarises the k values obtained for both models.

Table 5.17 Values of k obtained for CSTR and Wehner and Wilhelm models at each stage of the process performance evaluation (T = 25°C).

Configuration		CSTR		Wehner and Wilhelm
		k-$_{CODt}$ (h^{-1})	k-$_{CODf}$ (h^{-1})	k-$_{CODt}$ (h^{-1})
HBAP	1	0.080	0.064	0.054
	2	0.125	0.095	0.086
	3	0.094	0.085	0.073
MPAP	1	0.144	0.055	0.078
	2	0.287	0.243	0.142
	3	0.365	0.351	0.193
AP	1	0.083	0.024	0.059
	2	0.071	0.095	0.059
	3	0.102	0.136	0.084

The δ values from the hydrodynamic study were used to estimate the values of *k* for COD_t in the Wehner and Wilhelm model. Table 5.17 shows that the MPAP had the highest *k* values for both COD_t and COD_f. The average value of *k* improved with increases in the hydraulic loading rate. This suggests that contact between biomass and substrate must have been gradually enhanced which in turn increased the substrate degradation rate. Based on the mass transfer concepts discussed by Pavlostathis and Giraldo-Gomez (1991), it may be argued that the increase in the overall first-order reaction constant (*k*) obtained in this study was due to an improved mass transfer process from the bulk liquid to the bioflocs. The increasing upflow velocity in the mixing chamber of the MPAP may have influenced positively the transport of substrate towards the biomass aggregates. Brito and Melo (1999) found that transient variations in the upflow liquid velocity imposed on an anaerobic biofilm increased the mass transport by 20% on average. These authors argue that periodic changes in the bulk fluid velocity can be used as a tool to increase the transport of soluble substrates towards and inside anaerobic biofilms. Nonetheless, further research is needed to support this argument and to quantify the influence of liquid upflow velocity in mass transfer. Besides, a more controlled experimental setting would be desirable to carry out this sort of studies.

The *k* values for both COD_t and COD_f in the other AP were lower in comparison to the figures found for the MPAP. This is logical since COD_t removal efficiencies in the HBAP and the AP were always lower than in the MPAP. The values of *k* for the HBAP suggest that its best operation condition was during the second stage (HRT = 18 h). Although the values of *k* for the AP suggest a degradation rate similar to that in the HBAP, the correlation between experimental and predicted effluent COD_t values is lower in the former. Thus, it is again confirmed that conventional AP are not able to withstand hydraulic and organic loading rates higher than those given in Table 2.3 as recommended by Mara *et al.* (1992).

The figures in Table 5.17 show that Wehner and Wilhelm model yielded smaller values of *k* compared to the CSTR model. The differences are greater in the *k* values for the MPAP whilst for the other two AP the discrepancies are smaller. This together with the correlations presented below suggest that the Wehner and Wilhelm model yields better estimates of the first-order reaction constant k, in those reactors with more arbitrary flow patterns.

Equations 5.7 to 5.9 are the adjusted models for the prediction of effluent COD_t values at each AP configuration. The least-squares linear regression models with the

best fit are given together with either the adjusted CSTR or Wehner and Wilhelm models. The linear regression equations represent the correlation between experimental and predicted effluent COD_t figures for the respective model.

Model for HBAP

$$\frac{S_e}{S_o} = \frac{4ae^{1/2\delta}}{(1+a)^2 e^{a/2\delta} - (1-a)^2 e^{-a/2\delta}} \qquad (5.7)$$

$a = \sqrt{1+4k\theta.\delta} = \sqrt{1+0.34\theta\delta}$, $k = 0.085\ h^{-1}$

$COD_{e\text{-}pred} = 1.1781 COD_{e\text{-}exp} - 37.44$

$R^2 = 0.857$

Model for MPAP

$$S_e = \frac{S_o}{1+0.265\theta}, \qquad k = 0.265\ h^{-1} \qquad (5.8)$$

$COD_{e\text{-}pred} = 0.8771 COD_{e\text{-}exp} + 12.189$

$R^2 = 0.893$

Model for AP

$$\frac{S_e}{S_o} = \frac{4ae^{1/2\delta}}{(1+a)^2 e^{a/2\delta} - (1-a)^2 e^{-a/2\delta}} \qquad (5.9)$$

$a = \sqrt{1+4k\theta.\delta} = \sqrt{1+0.27\theta\delta}$ $k = 0.067\ h^{-1}$

$COD_{e\text{-}pred} = 1.0146 COD_{e\text{-}exp} - 3.3097$

$R^2 = 0.789$

Equations 5.7 to 5.9 show that the dispersion flow model with first-order kinetics described best the performance of the HBAP and the AP, whereas the CSTR model with first-order kinetics described more accurately the performance of the MPAP. It is worth noting that the *k* values obtained for the MPAP are comparable to the *k* values found for the UASB treating the same wastewater under the same environmental conditions. This again confirms one of the characteristics of high-rate anaerobic reactor found in the pilot-scale AP with a UASB-like mixing compartment.

Finally, the raw data and details of the statistic correlations are given in Appendix II in the file PILOT-SCALE-EXP\EXPERIMENT-III. Some of the results presented and discussed in this Chapter have been published elsewhere. The summary page of these publications can be seen in Appendix III.